

UNIVERSITY OF TWENTE

MASTER THESIS

Design of an Electro-Hydrostatic Actuated Ankle-Foot Orthosis

FACULTY OF ENGINEERING TECHNOLOGY
DEPARTMENT OF BIOMECHANICAL ENGINEERING

Author:
Jesús Jiménez Palao

Examination committee:
Dr. A. J. Veale
Dr.ir. D. Dresscher
Prof.Dr.Ir. H. van der Kooij

Document number:
BW-643

November 30, 2018

Abstract

This report presents the development of a research tool for the Biomechanical Engineering (BME) department of the University of Twente. The main goal of the presented project is to develop an hydrostatic actuated ankle exoskeleton. A frontal actuated ankle exoskeleton with a passive return was designed. The device counted with two hydraulic cylinders to assist plantarflexion and two mechanical springs as return elements. Once finish the physical prototype was tested using two different platforms. One platform consisted of a testing leg with digital force and motion sensors, that was connected to a hydrostatic input stage. The other had a manual pump with a digital force an analog pressure sensor.

Results obtained of the device's range of motion (ROM) showed that it is capable of reaching approximately 80° of total ROM, from which a maximum dorsiflexion angle of 24° and a maximum plantarflexion angle of 56° is reached. Furthermore, while performing a maximum stress test, it was found that the device can withstand a maximum ankle torque of 115.9 Nm.

In addition, the device was able to reach an ankle angular velocity of 113.16 deg/s. In total four of eight requirements set in this project were achieved. From this, the requirements that were not meet are the maximum exoskeleton weight, minimum actuation torque, minimum actuation velocity and the pain pressure threshold (PPT) for different areas of the lower limb.

In particular, to reach the minimum actuation torques for the different human movements the device structural stability needs to be improved. In the case of the weight, it is expected that by doing an optimization for lighter and stronger materials the total device mass can be further reduced. Due to equipment limitations, (1) it was neither possible to prove if the device's actuation can reach the minimum gait velocity requirements nor (2) if the device applied a significant pressure to the testing leg. Hence, to prove the speed and pressure requirements, it would be necessary to obtain small strain gauge sensors and a suitable input stage.

In conclusion, the device presented in this report is a promising solution to increase the ROM found in common ankle exoskeleton designs and it is a valuable reference to create new and compact devices that are able to perform different human movements.

Contents

Abstract	i
1 Introduction	1
1.1 State of the art	2
1.1.1 Pneumatic actuation	2
1.1.2 Hydraulic actuation	5
1.1.3 Electrical actuation	8
1.2 Project goals.	11
1.3 Design requirements	12
2 Concept design	14
2.1 Analysis description	14
2.2 Results	16
2.3 Conclusions	22
3 Prototype design	23
3.1 Orthosis body selection	23
3.2 Detailed design	26
4 Bench test	29
4.1 Equipment	29
4.1.1 Testing leg platform	29
4.1.2 Input stage	30
4.1.3 Manual pump platform	31
4.2 Experiments using the manual pump.	32
4.3 Experiments using the testing leg	33
4.3.1 Hanging leg experiment.	33
4.3.2 Stepping leg experiment.	34
4.4 Results	35
4.4.1 Range of motion	35
4.4.2 Exoskeleton's cylinder velocity	37
4.4.3 Forces	38
4.4.4 Results vs requirements	41

5 Discussion	42
5.1 Interpretation of results	42
5.1.1 Range of motion	42
5.1.2 Exoskeleton's cylinder velocity	43
5.1.3 Forces	43
5.2 Limitations	44
5.3 Recommendations	45
6 Conclusion	46
A Requirements notes	51
A.1 Range of motion	51
A.2 Weight	51
A.3 Torques	52
A.4 Stair dimensions	52
A.5 Design dimensions	52
A.6 Pressure pain threshold	54
A.7 Minimum angular velocity	54
A.8 Degrees of freedom	55
B Concept design analysis equations	57
B.1 Concept 1 equations	57
B.2 Concept 2 equations	58
B.3 Concept 3 equations	58
C Orthosis design process	59
C.1 Morphological chart-functions and solutions description	59
C.2 Hinges FME Analysis	61
C.3 Prototype's technical drawings	63
D Experiments illustrations and data	81
D.1 Manual pump test data	81
D.2 Range of motion illustrations	82

1 | Introduction

In the latest years, new and improved devices for gait rehabilitation have been created [1, 2, 3]. The reason is that the number of people that develop muscle weakness due to medical conditions such as stroke has been increasing [4]. The majority of gait rehabilitation devices are designed to assist the ankle joint, as studies have shown that most of the positive energy required for walking is produced in this joint [5].

To create an optimal assistive orthosis, many factors need to be considered. First of all, the weight of the device should be kept as low as possible, as any additional weight to the user's body will result in an increase of energy cost that can detriment the user's experience [6]. Another important factor related to the device's weight is the design of the device's structure. The structure should not interfere with the natural movement of the body joints, nor be uncomfortable to wear for the user.

Above all the most important factor to consider is the actuation method, taking into account both the force generated by the actuator and its synchronization to the gait cycle of the subject. Otherwise, the provided assistance would not be efficient or it could even be detrimental to the current health state of the person [7].

Today, the most common actuation principles used for ankle exoskeletons are electrical, hydraulic and pneumatic. Hydraulic actuators have the highest power-to-weight ratio, making them a great option for the development of limb exoskeletons [8]. However, they are limited by their dependence on an external fluid supply and the complexity of their pump and valves configuration. Luckily, in recent years new actuators that combine the best properties of the common actuation methods have arrived. A clear example is the electro-hydrostatic actuator developed by K. Staman et al. at the University of Twente [9]. This device conserves the attractive features of conventional hydraulic systems without using pumps and valves. Hence, it is easier to adapt to a wider variety of tasks.

The purpose of this report is to describe the design process that was done for the fabrication of an assistive ankle exoskeleton prototype with a single degree of freedom (DOF) and an electro-hydrostatic actuation. The reason, a single DOF is used is to simplify the overall design of the ankle exoskeleton. It is acknowledged that by doing so the overall user comfort will be reduced, however, it still needs to be investigated how this decision affects the final results of this device implementation.

1.1 State of the art

In this section, the current state of the art in ankle exoskeletons classified by their actuation principle is presented. In addition, a summary of the most important features of each exoskeleton is provided at the end of the section in Table 1.1.

1.1.1 Pneumatic actuation

Neuromechanics-based powered ankle exoskeleton

Researchers K. Z. Takahashi et al. created in 2015 a custom lightweight tethered ankle exoskeleton to assist walking in post-stroke patients [1]. The interesting feature of this device is its *proportional myoelectric propulsion* (PMP) control algorithm. This algorithm allowed the exoskeleton to supply a plantarflexion moment proportional to the paretic soleus electromyography (EMG) signal measured during the phase of stance when the anterior-posterior ground reaction force was greater than 0 (Figure 1.1).

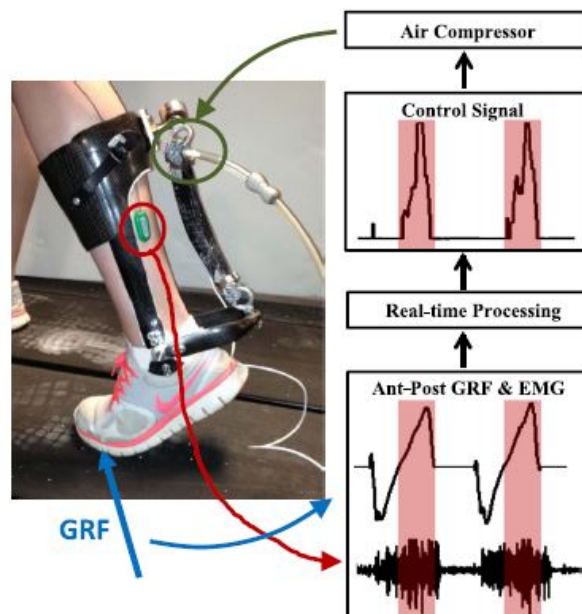


FIGURE 1.1: Illustration of the proportional myoelectric propulsion (PMP) powered exoskeleton [1].

Moreover, the exoskeleton has a relative light structure (0.532 ± 0.072 kg) made of a custom-fitted carbon fiber. The device performs plantar-flexion with an artificial pneumatic muscle that is attached along the posterior shank.

Portable Powered Ankle-Foot Orthosis

Pneumatic actuated exoskeletons are not normally found in untethered configurations. However, thanks to new technological developments scientist are now able to create less-bulky autonomous systems. One example is the Portable Powered Ankle-Foot Orthosis (PPAFO) illustrated in Figure 1.2 [10].

The PPAFO developed by Z. Wang et al. in 2016 is a fairly new device with the ability of providing bidirectional-assistive torque at the ankle joint. To generate this torque, the device uses a portable pneumatic power supply and a custom-made gear rack. Bench-top trials have shown that the device is capable of generating up to 32 Nm torque output at an operating pressure of approximately 7.6 Bar. With a weight of 0.68 kg and a ROM of 55° (plantar-dorsiflexion distribution not specified), this device seems to be promising. However, its performance during gait has not been tested in real subjects yet.



FIGURE 1.2: Back and side view of the PPAFO exoskeleton [10].

Bio-inspired soft wearable exoskeleton

One interesting approach for a pneumatic actuated exoskeleton design is the bio-inspired soft wearable robotic exoskeleton developed by Y.L. Park et al. in 2014 [3]. The main attribute of this device is that it uses four pneumatic artificial muscles to mimic the morphology and the functionality of the biological muscle-tendon-ligament structures of the ankle joint.

As can be seen in Figure 1.3 three actuators are located anteriorly to the shank for dorsiflexion, inversion, and eversion, and one is located posteriorly for plantarflexion. Its four actuators provide it with a significantly small ROM of 25° (12° plantarflexion, 13° dorsiflexion).

Moreover, the design of the exoskeleton is divided into three major groups: the base layer (containing the foot, ankle, and knee braces) where the actuation forces are transmitted to the lower limb, the actuation (artificial muscles, tendons, and ligaments), and the sensors layer (strain, IMU and pressure sensors).

This device has been tested with humans for seated motion and it has shown potential to be used in active assistance for ankle rehabilitation. Nevertheless, the device has not been tested yet in human gait and its dependency of using an external air source for the pneumatic muscles does not make it suitable to be used as an autonomous device.

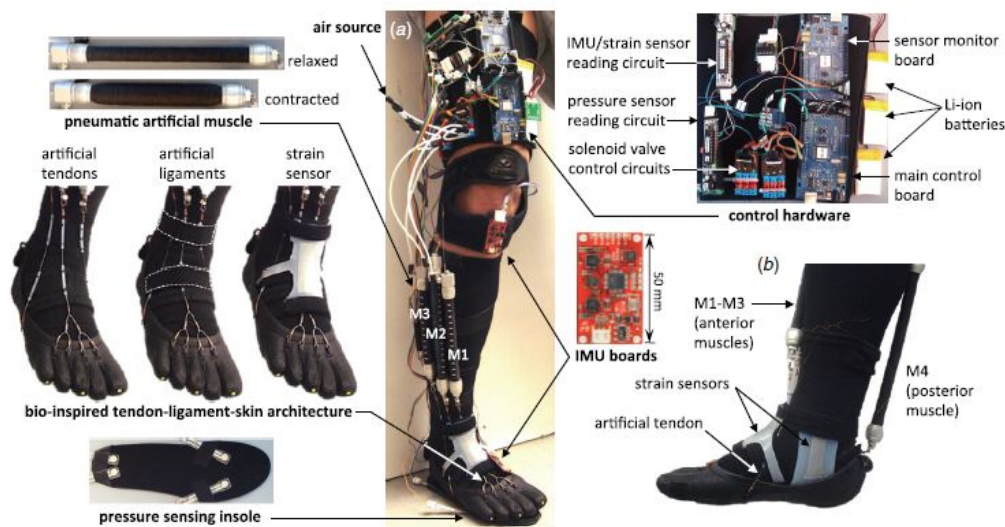


FIGURE 1.3: Illustration of the whole design of the bio-inspired ankle exoskeleton. a) front view b) side view [3].

1.1.2 Hydraulic actuation

Although hydraulic actuators have obtained the highest power-to-weight ratios in the last few years, little effort has been put on using this technology for ankle exoskeletons. This is mainly because hydraulic systems tend to be more complex to design compared to more traditional approaches as an electronic actuation [8].

Berkeley Lower Extremity Exoskeleton

The first successful autonomous hydraulic actuated exoskeleton was developed back in 2005 by the Berkeley Robotics and Human Engineering Laboratory at the University of California [11]. The Berkeley Lower Extremity Exoskeleton (BLEEX) is composed of two powered anthropomorphic legs, a power supply and a backpack-like frame that can be used to mount a variety of heavy payloads (Figure 1.4). Its design is almost anthropomorphic and it has seven DOF per leg of which three are at the ankle.

In addition, it uses double-acting linear hydraulic actuators to actuate four of its seven DOF (flexion/extension at the ankle) and it has a total power consumption of 1143W. The last results of BLEEX showed that it could support 75 kg walking at speeds up to 1.3 m/s. Overall the BLEEX was a promising and revolutionary device at its time, however, it still had a long way of improvement to surpass its limitations due to its bulky and heavy components.

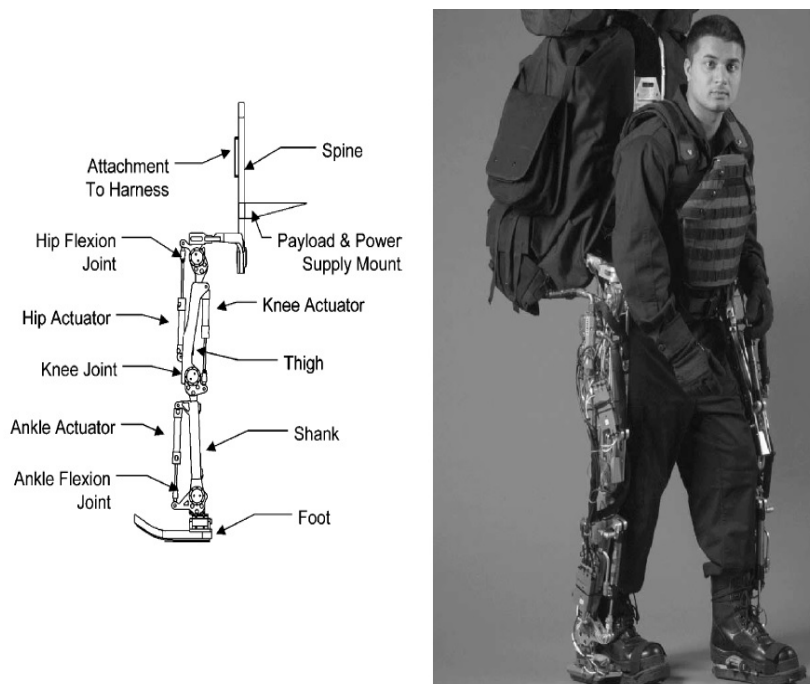


FIGURE 1.4: From left to right: the simplified model of the leg exoskeleton and participant wearing it [11].

Electrohydraulic Orthosis

Another example of a hydraulic actuation exoskeleton is the Electro-Hydraulic Orthosis (EHO) developed in 2008 by M. Noël et al. [12]. As illustrated in Figure 1.5 this tethered device uses a hybrid drive system composed of two pneumatic cylinders connected reciprocally by low mass plastic pneumatic hoses.

The master cylinder is driven by an electric motor while the slave cylinder is attached to the ankle exoskeleton. The motor used to drive the master cylinder is a brushless rotary motor coupled to a planetary gearhead with a ratio of 3:1. The motor can deliver a continuous torque of 70 Nm and a peak torque of 98 Nm at the output of the gearbox.

The exoskeleton is made of an aluminum structure and has an upright length of 0.30 m. The orthosis is made to have a certain range of adjustability to be fit into different subjects shank sizes as also for it to be interchangeable between the leg and right feet. The system uses a typical PID controller.

Furthermore, The system can change between torque (load cell) or position (optical encoder) control in real time through a software switch. The total mass of the orthosis alone is of 1.70 kg, and it has a single DOF in the sagittal plane with a total ROM of 47°. The device has been used solely as a research tool to investigate human gait. Hence, its potential to assist patients with walking impairment still needs to be tested.

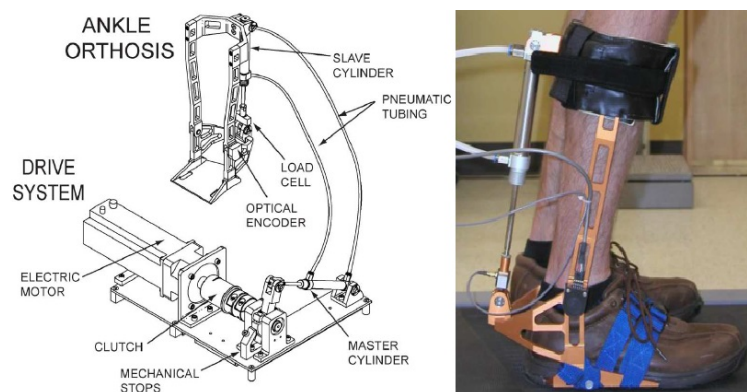


FIGURE 1.5: From left to right: Illustration of the actuation system of the EHO and the side view of the exoskeleton [12].

Hydraulic ankle-foot orthosis

A more recent autonomous device known as the Hydraulic Ankle-Foot Orthosis (HAFO) has shown great improvement in reducing the dimension and weight of hydraulic actuated exoskeletons. The device developed by B. Neubauer et al. in 2016 has a total weight of 3.30 kg (from which 0.97 kg are from the ankle actuator, 2.16 Kg from the power supply, and the rest of the weight comes from cushion and hoses) and it is capable of delivering up to 60 Nm during a simulated gait test (No human participation) [13].

The HAFO is divided in two sections, a hydraulic power supply at the waist and hydraulic actuators at the ankle. The two sections are connected by a pair of thin hydraulic hoses. The power supply comprises a battery, an electric motor, a hydraulic pump, and a set of valves while the actuators are two pairs of unidirectional pull-pull hydraulic cylinders actuators.

The ankle component is composed of a shin support, a foot plate, and medial and lateral actuators that move the ankle through sagittal plane dorsi-and-plantarflexion (Figure 1.6). The foot plate distributes the torque generated by the actuators on the shoe and the foot. The foot is secured to the plate using a conventional shoe that is two sizes larger than the user's shoe size.

The pump has a maximal operation angular velocity of 2000 rpm and a maximum operating pressure of 138 bar. Although the device has a lighter and compacter design compared to equivalent electromechanical versions, it still could not deliver the speed and torque requirements for gait.

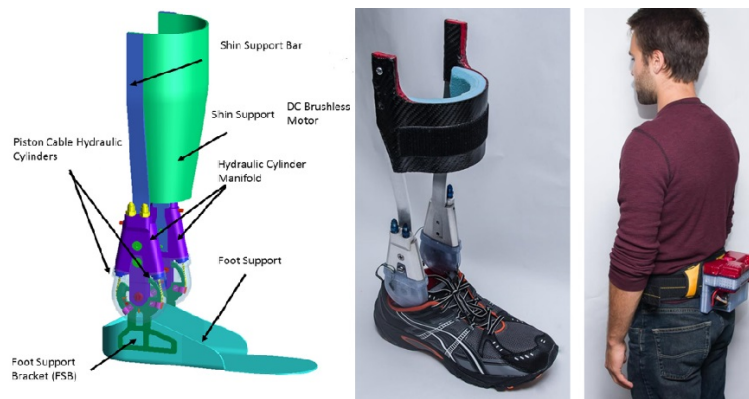


FIGURE 1.6: HAFO Component description, physical model and power source [13].

1.1.3 Electrical actuation

Portable ankle-foot orthosis

One interesting approach for an electrically actuated exoskeleton is the Portable Ankle-Foot Orthosis (P-AFO) developed by Yang Bai et al. in 2015 [2]. With a length of 0.245 m, this relatively small device is attached to the leg using straps that surround the calf area and a plate that rests under the heel of the user. Its main characteristic is its actuation method, which is located on the frontal side of the leg (Figure 1.7). The actuation system is composed of a high accuracy servo motor and a transmission.

Likewise, the transmission is composed of a lightweight but powerful harmonic drive, bevel gear, and synchronous belt units that allow the device to give plantar and dorsiflexion assistance for a ROM of 30° (12° for plantarflexion, 18° for dorsiflexion). Although only wearing and motion experiments have been carried out for this device, its results show that it is a promising solution to be used in walking rehabilitation.

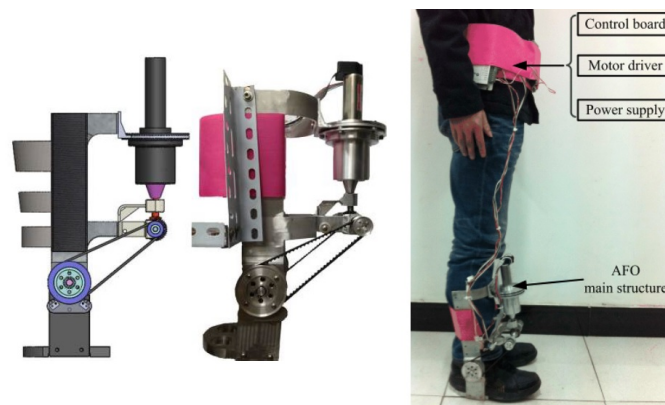


FIGURE 1.7: From left to right: exoskeleton CAD drawing, physical model, and demonstration of participant wearing it [2].

MIT's Autonomous exoskeleton

Another example is the autonomous exoskeleton developed by Mooney et al. in 2014 [14]. This device uses a unidirectional electrical motor to wind a cord attached to a pair of fiberglass struts located laterally to the shank. The struts are then attached to the bottom of a boot and when the actuator winds the cord a force is transmitted to the struts, which produce a torque that acts at the ankle joint (Figure 1.8).

This exoskeleton successfully improved the energy cost of walking in an experiment where users were using an additional load of 23 kg. The total observed metabolic cost reduction compared to the control condition (not wearing the exoskeleton) was of $8 \pm 3\%$, which is impressive considering that it is an autonomous device [14].



FIGURE 1.8: MIT Autonomous exoskeleton [14].

Achilles ankle exoskeleton

Illustrated in Figure 1.9 is the Achilles exoskeleton developed by C. Meijneke et al in 2014. This device consists of two boot parts which individually have an electric motor, sensors (pressure sensor, incremental encoder) and a mechanism to transfer power to the human [15]. The boot parts are designed to exert a torque around the ankle which is produced by a motor (Maxon-EC22 4 pole motor) with a series elastic actuator (SEA), a ball-screw spindle (SFK-SH6x2), and a leaf spring. This actuation system could exert theoretically 192 W of power and a torque of 78.54 Nm around the ankle.

In addition the weight of the exoskeleton is 1.5 kg per foot. The backpack that contains the power sources has a mass of 5.2 kg. The system alone could deliver enough power to fit the torque requirements of gait, and in bench-tests it reached a peak power of 80.2 W [16].

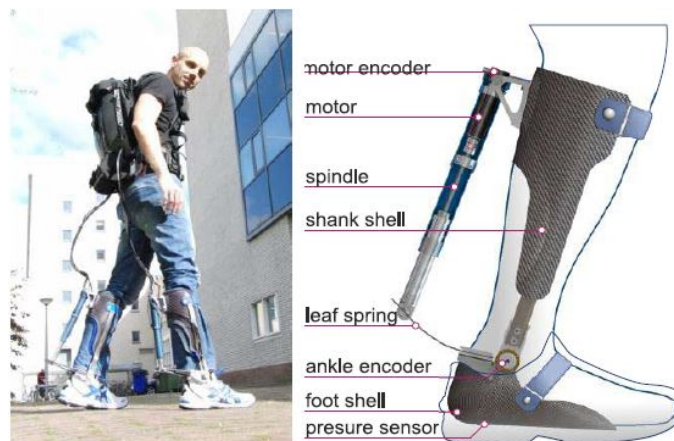


FIGURE 1.9: Illustrations of the Achilles exoskeleton with the backpack supply worn by a subject (left) and description of the components of the exoskeleton (right) [16].

Alpha and Beta exoskeltons

The last three mentioned devices are autonomous, meaning that the actuation and the power source are carried by the user. However, there are also other types of exoskeletons that have their power source and actuation separated. These devices are more commonly known as tethered exoskeletons. These devices are used mostly for rehabilitation or research as they are limited by the area where the power source is located. Nevertheless, thanks to having an external actuation, the weight of the carried exoskeleton can be kept really low without sacrificing force.

Examples of such devices are the Alpha and Beta models developed by K. A. Witte et al. in 2015 [17]. The Alpha exoskeleton was designed to provide compliance in selected directions while the Beta was designed to have a compacter structure. The actuation for both models is done by an off-board electrical motor and a real-time controller. The motor transmits the mechanical power through a flexible Bowden cable connected to the exoskeleton's end-effector. As illustrated in Figure 1.10 each exoskeleton is attached to the leg at points located in the heel, the shin below the knee, and the ground beneath the toe.

These exoskeletons are highly suitable for rehabilitation or research purposes due to a relatively small weight of 0.835 and 0.875 kg for the Alpha and Beta models, respectively. They have been capable of delivering an average peak plantarflexion torque of 80 Nm and 87 Nm, respectively, in controlled walking. In addition, their wide ROM (30° plantarflexion and 20° dorsiflexion) makes them more than suitable to assist in walking.

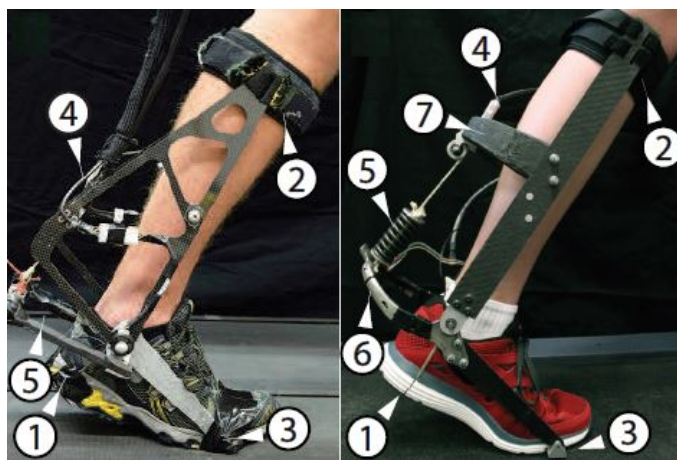


FIGURE 1.10: From left to right: Alpha and Beta model. The Alpha design has a string under heel(1), a strap to assure the shin (2), a hinged plate embedded in the shoe (3), a shank frame where the Bowden cable conduit is attached (4) and a series spring (5). In addition to (1-5), the beta design has a titanium ankle lever wrapping behind the heel (6) and a hollow carbon fiber Bowden cable support(6) [17].

Summary

To provide a fast and easy method to compare the individual characteristics of the aforementioned devices, the Table 1.1 was created.

TABLE 1.1: Exoskeletons specifications summary

Actuation method	Device name/year	Advantages	Limitations	Exoskeleton weight	ROM	DOF	Actuation torque
Electrical	Portable ankle-foot orthosis, 2015 [2]	Compact, strong structure, autonomous	Bulky	-	12° plantarflexion, 18° dorsiflexion	1 active	-
	MIT Autonomous exoskeleton, 2014 [14]	Ergonomic design, autonomous	Control need improvement	1.35 kg	-	1 active	-
	Achilles exoskeleton, 2014 [15] [16]	Lightweight, ergonomic, autonomous	Limited ankle range of motion	1.5 kg	-	1 active	78.54 Nm
	Alpha exoskeleton, 2015 [17]	High power, Lightweight, high band-width	Non-autonomous, not adjustable design, it has a larger medial and posterior protrusions which may affect gait	0.835 kg	30° plantarflexion, 20° dorsiflexion	1 active	80 Nm (peak average measured torque)
	Beta exoskeleton, 2015 [17]	High power, lightweight, high band-width	Non-autonomous, not adjustable design	0.875 kg	30° plantarflexion, 20° dorsiflexion	1 active	87 Nm (peak average measured torque)
Pneumatic	Neuromechanics-based powered ankle exoskeleton, 2015 [1]	Lightweight, ergonomic design	Non-autonomous, dorsiflexion is not assisted	0.5323± 0.072 kg	-	1 active	-
	Bio-inspired ankle exoskeleton, 2014 [3]	Bio-inspired actuation system, complete soft structure	Non-autonomous, complex actuation	-	12° plantarflexion, 13° dorsiflexion	2 active	-
	Portable powered ankle-foot orthosis, 2016 [10]	Lightweight, Autonomous	Bulky	0.68 kg	55° (Total range, not specified for plantar-dorsiflexion)	1 active	32 Nm (at approx. 7.6 Bar)
Hydraulic	BLEEX, 2006 [11]	Autonomous, can carry payload, high propulsion and pulling force	Bulky, heavy	-	45° flex ion, 45° extension, 20° adduction, 20° abduction	1 active 2 passive	150 Nm, (approx.values of torque for push motion) 190 Nm (approx.values of torque for pull motion)
	Electro-hydraulic actuated ankle foot orthosis, 2008 [12]	Adjustable design, can apply controlled force fields	Non-autonomous	1.7 kg	47° (Total range, not specified for plantar-dorsiflexion)	1 active	-
	Hydraulic ankle-foot Orthosis, 2016 [13]	Autonomous, lightweight, ergonomic	Does not fulfilled the minimum requirements for gait, limited pump speed and force	0.97 kg	50° plantarflexion, 20° dorsiflexion	1 active	60 Nm

1.2 Project goals

The main goal of this project is to design a device that can perform the minimum requirements necessary to perform walking, stair climbing, and sit-to-stand (STS) motion. It is expected that the device is used as a research tool at the University of Twente to investigate rehabilitation methods for patients with lower leg muscles weakness. In addition, a sub-goal of this project is to investigate the advantages and disadvantages of using an electro-hydrostatic actuation in an ankle-foot orthosis (AFO).

1.3 Design requirements

The current state of the art on ankle exoskeletons, provided a general idea on the points to focus to define the design specifications. For instance, an important factor is that the device should be able to perform the necessary ROM for the desired motion. In this project, the device should cover the minimum range of plantar and dorsiflexion involved in walking, stair climbing, and the STS motion.

Another factor is the weight and body volume of the device. The device should be light, relatively compact and comfortable when it is worn and actively used. Above all, the most important thing is that the device is able to correctly assist the user's locomotion. In other words, the device should deliver enough torque and act fast enough to at least keep with the minimum pace of the desired motion.

Hence, considering the aspects mentioned above, the requirements list presented in Table 1.2 was defined. The values shown in Table 1.2 are based on the state of the art section as well as in the additional information presented in the notes in Appendix A.

TABLE 1.2: Requirements list

<i>Description</i>	<i>Specific values</i>	<i>Notes</i>
Exoskeleton range of motion	Total ROM: 55° Plantarflexion: 35° Dorsiflexion: 20°	A.1
Exoskeleton weight	Max : 1.5 kg	A.2
Min actuation torque for climbing, walking and STS motion	Min walking plantarflexion torque: 136 Nm Min walking dorsiflexion torque: 24 Nm Min stairs climbing plantarflexion: 132 Nm Min stairs climbing dorsiflexion: 3.2 Nm Min STS plantarflexion: - Min STS dorsiflexion: 67 Nm	A.3
Stairs dimensions in which the device needs to function	Stair riser dimension: 0.102- 0.178 m Min stair tread depth: 0.279 m	A.4
Maximum area dimensions for the orthosis design	Total height: 0.51 m (from the foot sole to the knee) Anterior leg space: 0.26 - 0.286 m (42 - 45 EU shoe size) Posterior leg space: 0.16 m (arbitrarily selected) External leg space: no specific limit. Max internal leg space: 0.20 m	A.5
Pressure limits for different lower leg areas	Max posterior lower leg PPT(Pain Pressure Threshold): 545 KPa Max anterior lower leg PPT: 416 KPa Max foot dorsum PPT : 360 KPa Max foot sole PPT: 240 KPa	A.6
Min. actuation speed for climbing, walking and STS motion	Min. walking plantarflexion angular velocity in the ankle joint: 150 deg/s Min. walking dorsiflexion angular velocity in the ankle joint: 55 deg/s Min. stair climbing plantarflexion angular velocity in the ankle joint: 60 deg/s Min. stair climbing dorsiflexion angular velocity in the ankle joint: 61.7 deg/s Min. STS plantarflexion angular velocity in the ankle joint: 20 deg/s Min. STS dorsiflexion angular velocity in the ankle joint: 25 deg/s	A.7
Total DOF	1 (sagittal plane)	A.8

As seen in Table 1.3, it is clear that there is not yet a device capable of meeting all the necessary aspects for a proper assistive ankle exoskeleton. Hence it is really important to aim to fulfill these requirements in order to generate a better device.

TABLE 1.3: Evaluation of the State of the art devices based on some of the main project's requirements

<i>Device name</i>	<i>Exoskeleton Weight</i>		<i>ROM</i>		<i>Min. actuation torque</i>	
	<i>Specs</i>	<i>Grade</i>	<i>Specs</i>	<i>Grade</i>	<i>Specs</i>	<i>Grade</i>
Portable ankle-foot orthosis [2]	-	-	12° PF 18° DF.	NS	-	-
MIT Autonomous exoskeleton[14]	1.35 kg	S	-	-	-	-
Achilles exoskeleton[15][16]	1.5 kg	S	-	-	78.64 Nm	NS
Alpha exoskeleton[17]	0.835 kg	S	30° PF 20° DF	NS	80 Nm	NS
Beta exoskeleton[17]	0.875 kg	S	30° PF 20° DF	NS	87 Nm	NS
Neuromechanics-based powered ankle exoskeleton[1]	0.5323 ± 0.072 kg	S	-	-	-	-
Bio-inspired ankle exoskeleton[3]	-	-	12° PF 13° DF	NS	-	-
Portable powered ankle-foot orthosis[10]	0.68 kg	S	55° (Total ROM)	?	32 Nm	NS
BLEEX[11]	-	-	45° PF 45° DF	S	150 Nm (Push) 190 Nm (Pull)	NS
Electro-hydraulic actuated ankle foot orthosis[12]	1.7 kg	NS	47° (Total ROM)	?	-	-
Hydraulic ankle-foot Orthosis[13]	0.97 kg	S	50° PF 20° DF	S	60 Nm	Ns

S = Sufficient , NS = Not sufficient, - = information not available, ? = no conclusion. There is not enough available information
PF= Plantarflexion, DF = Dorsiflexion

2 | Concept design

In this chapter, first, a numerical analysis to determine the optimal way of positioning the actuator of the exoskeleton is described. Second, a discussion about the results of this analysis is presented. Finally, the section ends with a conclusion about the chosen concept.

2.1 Analysis description

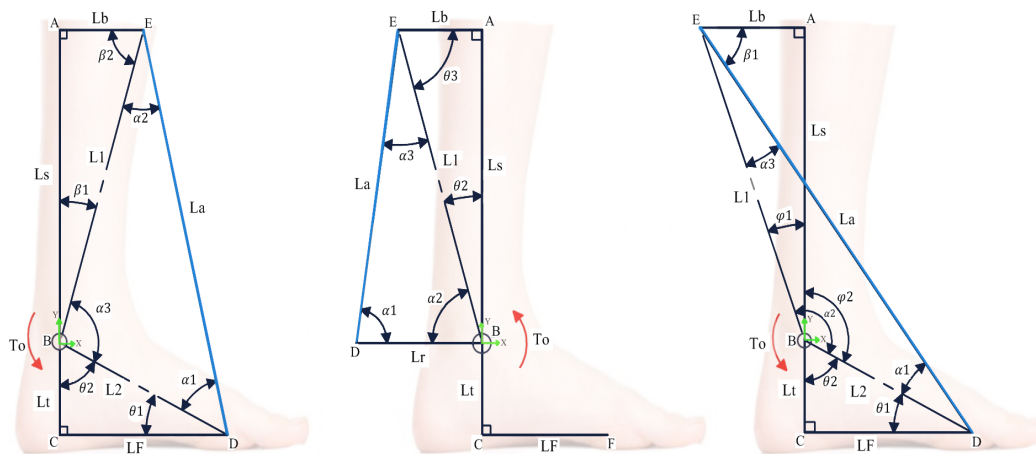


FIGURE 2.1: Numerical analysis concepts: from left to right, concept one, two and three.

For the analysis the three different structural concepts seen in Figure 2.1 were used:

- Concept one: Structure that allows fixing an actuator to the anterior side of the lower leg. The reason to consider this concept was that by locating the actuator in this position, a collision between the exoskeleton and a step when descending stairs can be prevented.
- Concept two: Common structure used in the design of ankle exoskeletons in which the actuator is located posteriorly to the leg. The reason to consider this structure was to see how do the other two concepts (concepts one and three) perform in contrast to the "standard" design of ankle exoskeletons.

- Concept three: Structure that has a top fixing point posteriorly to the leg and a bottom fixing point anteriorly to the leg. This concept was considered as an alternative solution for the stair descending problem.

To perform the numerical implementation the set of values shown in Table 2.1 was defined for the concepts joint lengths. The upper and lower limits of the values in Table 2.1 were based on the maximum lower leg measures of a single subject. Furthermore, for each concept trigonometrical equations (Appendix B.1, B.2, B.3) were obtained. These equations were used to determine the concepts internal angles and the parameters: moment arm (r), actuator length (L_a), actuator stroke (S_a), actuator's linear velocity (V_a) and actuator force (F_a).

Since a high actuator linear velocity is a normal limitation for hydraulic actuators, the parameters (1) actuator linear velocity and (2) moment arm were the first to be investigated. In this analysis, all possible combinations of the values shown in Table 2.1 were used in the concept's equations to evaluate the effect that each length variable had on the actuator's linear velocity and moment arm. Then with the obtained information the most relevant variables for controlling the moment arm and actuator linear velocity were determined.

For each concept, these variables were used to generate a single configuration with realistic measures based on a desired moment arm length. Finally using these configurations and the ankle torque and angle datasets from the book of D.A. Winter, the values (1) maximum and minimum moment arm, (2) maximum and minimum actuator length, (3) maximum actuator force, (4) maximum actuator linear velocity and (5) actuator stroke length were estimated to compare the concepts performance [18].

TABLE 2.1: Concept's lengths data

<i>Concept one</i>								Units
L_b	40	60	80	100	120	140	160	mm
L_f	40	70	100	220	150	180	210	mm
L_s	40	100	160	220	280	340	400	mm
L_t	40	50	60	70	80	90	100	mm
<i>Concept two</i>								
L_s	40	100	160	220	280	340	400	mm
L_s	40	100	160	220	280	340	400	mm
L_s	40	100	160	220	280	340	400	mm
L_s	40	100	160	220	280	340	400	mm
<i>Concept three</i>								
L_b	-40	-60	-80	-100	-120	-140	-160	mm
L_f	40	70	100	220	150	180	210	mm
L_s	40	100	160	220	280	340	400	mm
L_t	40	50	60	70	80	90	100	mm

2.2 Results

Concept one: variables effect on moment arm and actuator linear velocity

The numerical analysis of the concept length variables revealed that the contribution of variables L_s and L_t did not significantly affect the magnitude of the moment arm length. The reasons are: (1) there was a difference of less than 20% between the data obtained from the configurations using the maximum and minimum value of variable L_s , and (2) a difference of less than 3% between the maximum and minimum value for variable L_t .

Hence, to observe the possible magnitudes of the actuator moment arm, lengths L_s and L_t were set to their maximum values and all their respective remaining value combinations were analyzed. Figure 2.2 shows the effect of changing the length value of variables L_f and L_b for the configuration previously mentioned. It may seem the results on Figure 2.2 show that length L_b has a significant effect on the magnitude of the moment arm length, but its effect is almost equal to the one of length L_s . Hence, for this concept length L_f is the most important variable to modify the magnitude of the moment arm.

The results of the actuator linear velocity estimation shown in Figure 2.3 also reveal that the most relevant variable to modify the actuator linear velocity is the length L_f . This is expected, because the moment arm length is directly correlated to the actuator linear velocity magnitude. Hence, for the comparison between the concepts, variable L_f will be the determining factor in the selection of an adequate configuration.

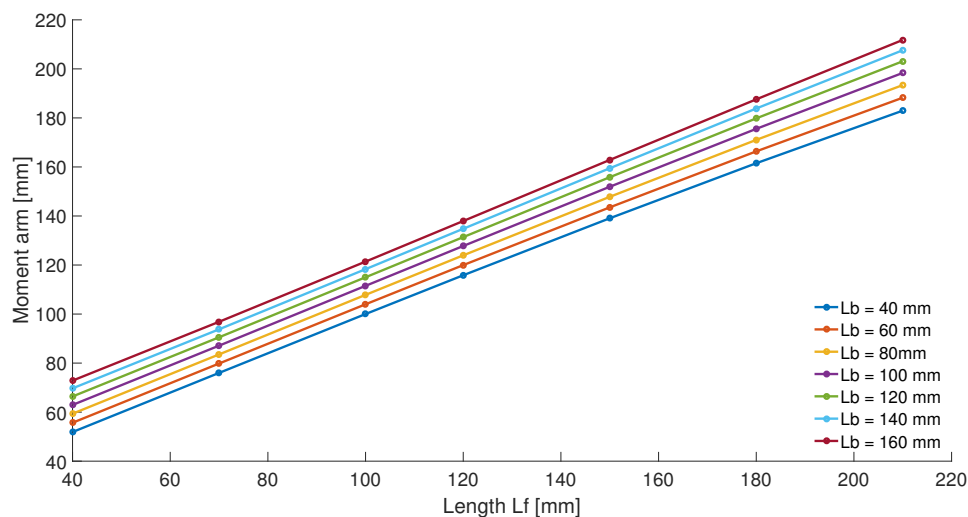


FIGURE 2.2: Moment arm change to different values of lengths L_f and L_b

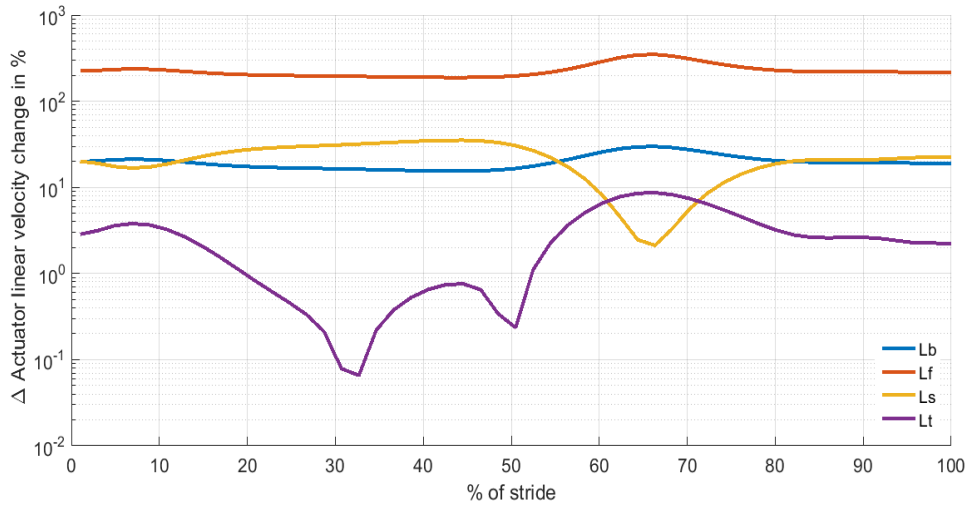


FIGURE 2.3: Effect of changing values for each length parameter on the actuator linear velocity. Lines represent the percentage values of the difference between the actuator linear velocity data obtained using the maximum and minimum length of each variable and the ankle joint angle of the maximum gait torque. So for L_f ,

$$\Delta V_{L_f} = (||v_{L_fmax}| - |v_{L_fmin}||) / |v_{L_fmin}| \cdot 100$$

Concept two: variables effect on moment arm and actuator linear velocity

The moment arm analysis of concept two reveals that length L_r is the most significant variable affecting the magnitude of the moment arm on this concept. As shown in Figure 2.4 an increase of length L_r produce an almost proportional increase of moment arm length. Also in Figure 2.4, at first sight, length L_s has a similar effect on the moment arm magnitude, however, this was not the case, because when length L_s increase, the effect of L_s on the moment arm decrease. It was expected that length L_b would be one of the variables that modified more the actuator moment arm, however, it was found that its effect is not significant enough, because there was only a change of 3% between the results obtained using different lengths L_b

Interestingly enough in contrast to the moment arm analysis, the actuator linear velocity analysis reveals a new insight into the effects of the length variables on this concept. This time not only length L_r remain an important variable to consider for the optimization of this concept, but as seen in Figure 2.5 the results also showed that length L_s is crucial for the selection of the actuator linear velocity. Hence, these two variables will be the determinants to obtain a configuration to be used in the concepts comparison.

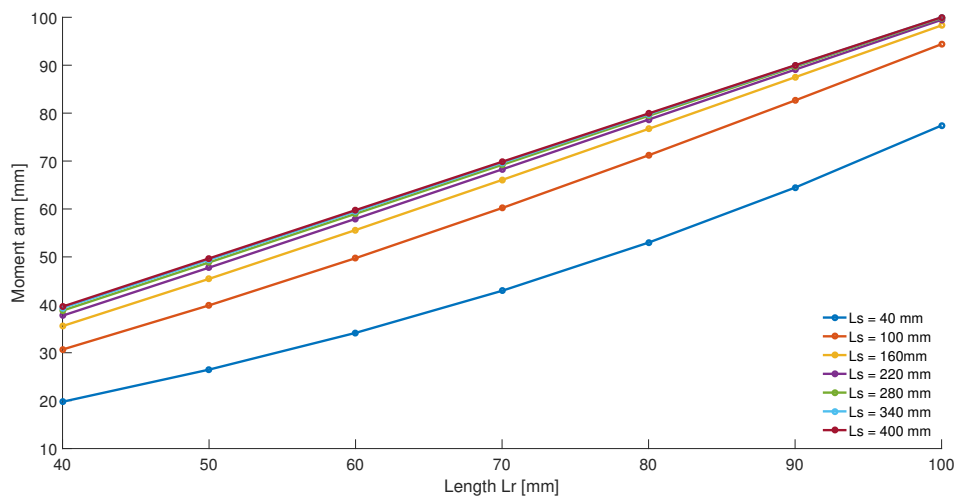


FIGURE 2.4: Moment arm change to different values of lengths L_r and L_b

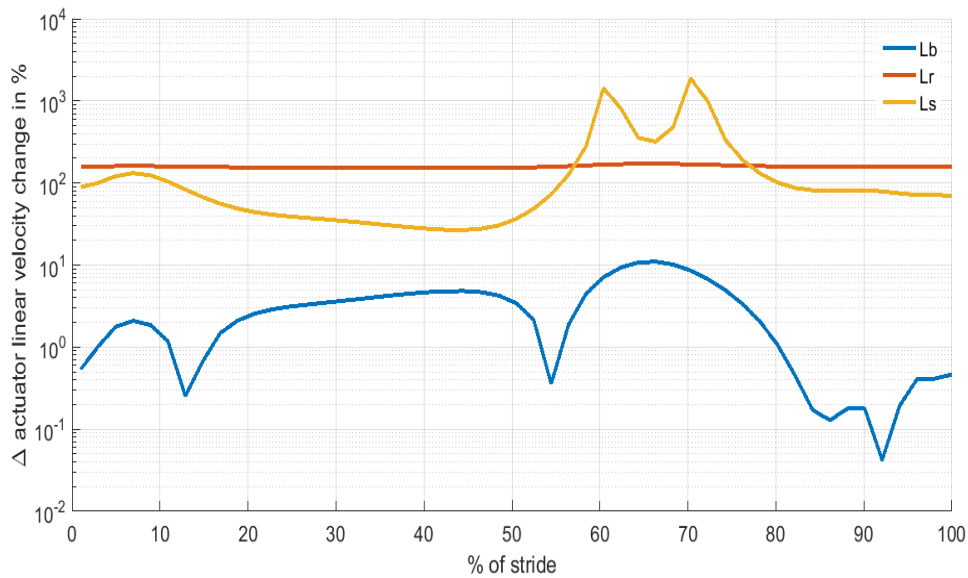


FIGURE 2.5: Effect of changing values for each length parameter on the actuator linear velocity. Lines represent the percentage values of the difference between the actuator linear velocity data obtained using the maximum and minimum length of each variable and the ankle joint angle of the maximum gait torque. So for L_f ,

$$\Delta V_{L_f} = (|v_{L_fmax}| - |v_{L_fmin}|) / |v_{L_fmin}| \cdot 100$$

Concept three: variables effect on moment arm and actuator linear velocity

The numerical results of the moment arm analysis showed that the most important variables to modify the magnitude of the moment arm were the lengths L_s and L_f , with this last having the greatest contributing overall. As illustrated in Figure 2.6. The moment arm length increases almost linearly with L_f . In contrast, variable L_s modifies the magnitude of the moment and changes the effect of the variable L_f from one case where the moment arm increases as L_f increases and another case in which the moment arm decreases as L_f increases.

As for the actuator velocity analysis it was found that both variables L_s and L_f have the greatest influence on actuator velocity (Figure 2.6). However, in contrast to the individual effect of this variables on the moment arm, the effect of both variables on the actuator linear velocity is almost the same. Hence, variable L_f is the dominant variable affecting both the actuator velocity and moment arm. So just as in concept two, values will be chosen for both variables to create a configuration which can be used to fairly compare the potential of this concept against the others.

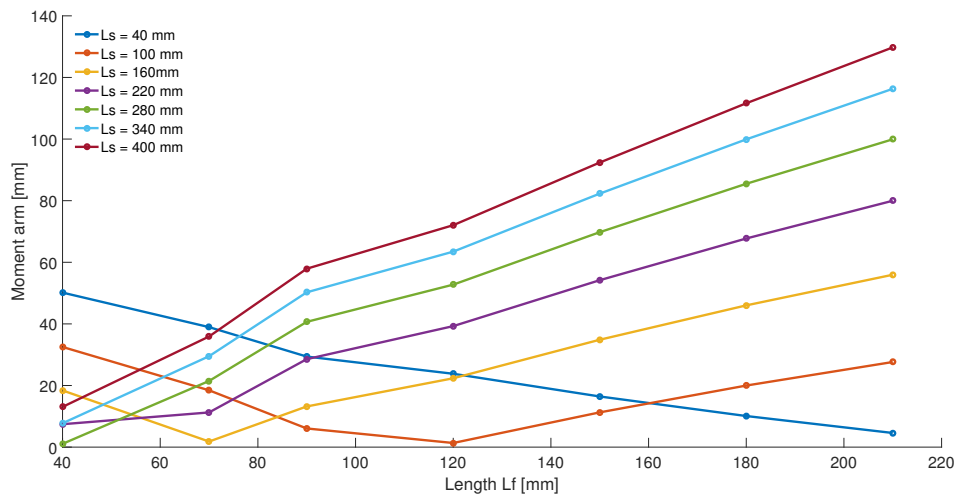


FIGURE 2.6: Moment arm change to different values of lengths L_f and L_s

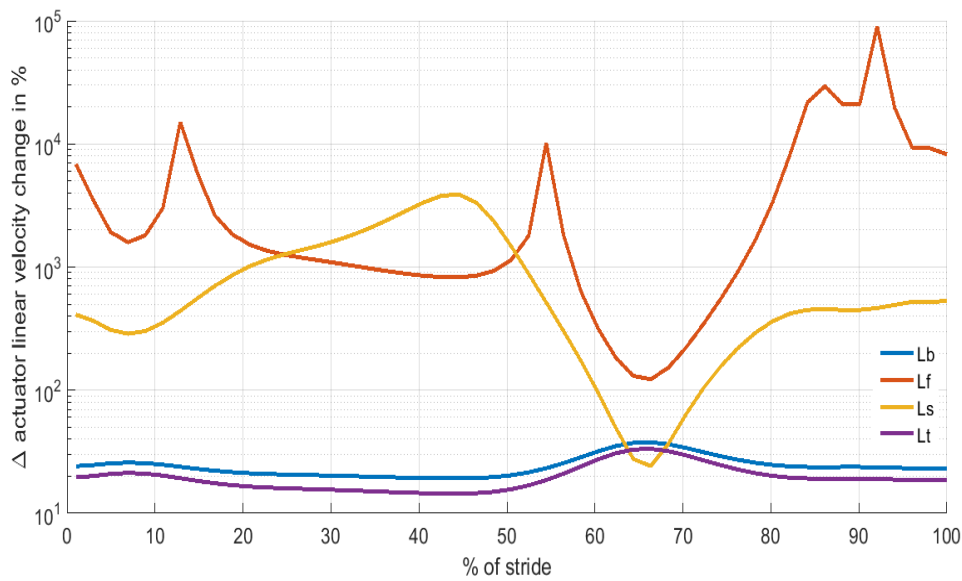


FIGURE 2.7: Effect of changing values for each length parameter on the actuator linear velocity. Lines represent the percentage values of the difference between the actuator linear velocity data obtained using the maximum and minimum length of each variable and the ankle joint angle of the maximum gait torque. So for L_f ,

$$\Delta V_{L_f} = (|v_{L_f \max}| - |v_{L_f \min}|) / |v_{L_f \min}| \cdot 100$$

Parameters analysis between concepts

After investigating the effects of the length variables on the moment arm, an arbitrarily moment arm length of 100 mm was chosen. The value of the moment arm was selected so that a reasonable structure for each concept is obtained. Then with the selected moment arm, for every concept a configuration that approximately reached this value was selected. In the configuration selection, the most important variables found in the previous sections were considered. Table 2.2 show the variables lengths of all concepts selected configurations. Finally, for each configuration, the parameters presented in Table 2.3 were obtained to compare and find which of the concept presented in this chapter has the best structure for the prototype design of the ankle exoskeleton.

TABLE 2.2: Parameters results for all concepts using an almost identical max moment arm length (r)

Concept	L_r	L_s	L_b	L_t	L_f	Units
#1	N/A	400	40	100	100	mm
#2	100	400	160	N/A	N/A	mm
#3	N/A	400	-40	100	120	mm

Looking at the results of Table 2.3 all concepts present a similar actuation force magnitude. This is expected since in each concept the moment arm was maintained approximately the same. In the case of the actuator linear velocity, the results significantly vary between all concepts. At first sight, it seems that concept two will be the less favorable of the three since it is the concept that obtained the highest value of actuator linear velocity.

As for the results of the maximum and minimum actuator lengths it was found that concept two is the concept with the overall smallest actuator size. This could be beneficial to create a compact device, however, finding an actuator of this size that accomplishes the actuator force and linear velocity obtained for this concept would be complicated.

Concept three obtained the longest actuator length, yet, it still remained inside the limitation area of the project requirements. Although there is a difference of about 19 mm between the maximum actuator length of concept three and one, their respective total stroke lengths are practically the same. As expected, concept two had the longest stroke length, however, in contrast to the difference in maximum actuator length, the stroke length did not greatly vary from that of the other concepts. Lastly, observing the minimum moment arm results, it can be noted that concept three obtained the shortest moment arm value. A short moment arm in concept three can be a problem, because the actuator would need to be too close to the leg which could result in a complex design.

TABLE 2.3: Parameters results for all concepts using an almost identical max moment arm length (r)

	<i>Concept one</i>	<i>Concept two</i>	<i>Concept three</i>	Units
$F_{a_{max}}$	1302.3	1302.4	1324.2	N
$V_{a_{max}}$	283.3	346.4	268.4	mm/s
$L_{a_{max}}$	528.3	421.2	547.8	mm
$L_{a_{min}}$	487.7	372.1	509.5	mm
S_a	40.6	49.2	38.3	mm
r_{max}	101.3	100	99.8	mm
r_{min}	55.3	86.6	47.9	mm

2.3 Conclusions

Electro-hydrostatic actuators just as hydraulic actuators are great delivering huge forces, however, because of that they tend to work at a relatively small actuation velocity. For that reason, the maximum actuator linear velocity is the crucial parameter in this analysis.

On the one hand, the results of Table 2.3 clearly show that concept two is not the best concept of the three. Because even when all concepts had approximately the same moment arm length and actuator force, concept two had by far the highest value of actuator linear velocity. Moreover, concept two is the only concept in which the actuator applies a pulling force to perform plantarflexion. In theory, this is an advantage since it resembles real muscle's dynamics, however, since the direction of action will be against gravity it is expected that there is going to be much more resistance in the actuator cylinders than in the other two concepts.

On the other hand, the results of concept one and three present almost identical values for all the parameters, with the exception of the maximum and minimum actuator length ($L_{a_{max}}, L_{a_{min}}$). The difference in actuator length does not seem to be really relevant as the value of stroke length (S_a) is almost the same in both concepts. Although the minimum moment arm value of concept three is slightly smaller than the one of concept one, in the case of concept three having such a small moment arm can be a problem, since not only finding a design that fit those dimensions is a complicated task but also because there could be instance that the device is in a mechanical singularity.

In the end it was decided that concept one would be a better choice because it is easier to work in the post-design of this concept, since both its actuation anchor points stay in one single plane (anteriorly to the shin) in contrast to concept three, which has one anchor point anteriorly to the shin and the other behind the calf. Aside from that, there seems not to be any advantage of using concept two instead of concept one, that would compensate the extra work on the later design stages.

3 | Prototype design

In this chapter, first, the process considerations to create a prototype of the orthosis body are explained. Later, a detailed design of the prototype and the list of its components are presented.

3.1 Orthosis body selection

In order to create an optimal design for the ankle exoskeleton, the morphological chart presented in Table 3.1 was created. The chart was generated considering the structural frame concept selected in Chapter 2. Moreover, the chart only covers the fundamental functions and solutions to create the structure that will interact with the human limb. A brief description of each function and the reasoning behind their respective solutions are described in Appendix C.1

TABLE 3.1: Morphological chart

Function	Solution 1	Solution 2	Solution 3	Solution 4	Solution 5
Fastener method	 velcro straps	 belt	 boa laces	 pressure buttons	 compression sleeve
Upper force distribution	 part(s) on the sides	 part(s) on the back	 part(s) on the front		
Lower force distribution	 foot top	 foot sole			
Shank/foot hinge	 one sided hinge	 double sided hinge			

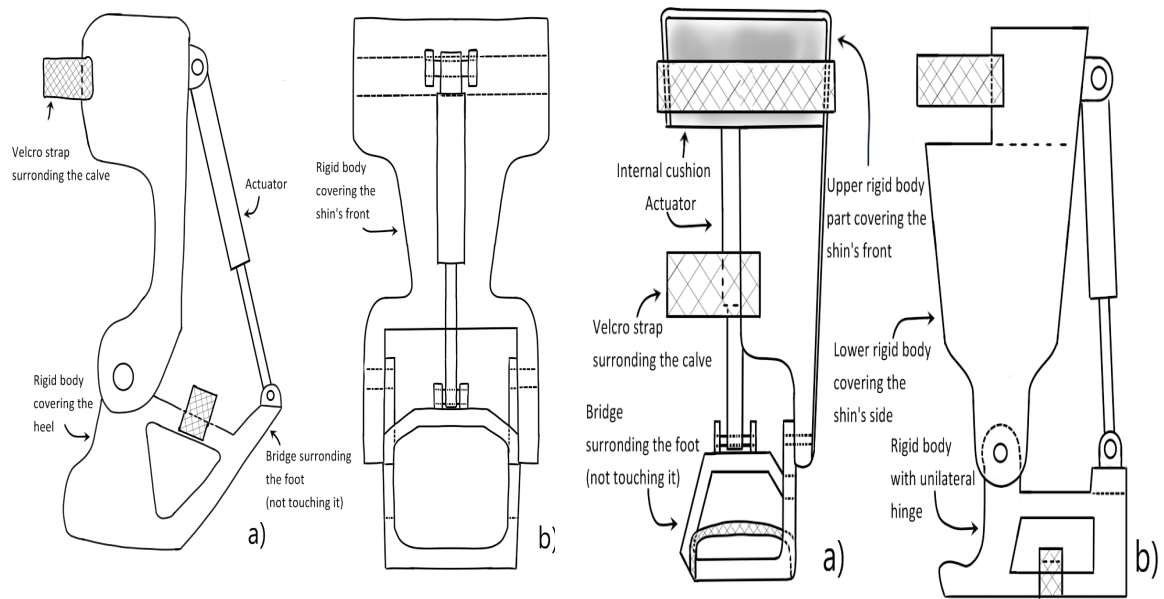
For the *fastener method*, it was decided that using velcro straps would be the best choice. The reason is that unlike boa laces and belts, velcro straps do not produce a significant discomfort in the lower leg. And although velcro straps tend to get loose due to wear, they can be easier adapted to different shin sizes in contrast to pressure buttons and compression sleeves.

In the function *upper-force distribution* only the solution one (part(s) on the sides) was not considered, because in contrast to the other two solutions, solution one does not provide any additional force distribution advantage, and only complicates the task of designing an anchor point for the actuator.

Furthermore, it was decided that the best option for the function *lower-force distribution* would be to use a body that equally spreads the force on the sole. This decision was done because the top of the foot is a really sensitive area that when pressure is applied without proper care, it can lead to discomfort or even pain. Lastly, all solutions of the function *shank/foot hinge* were considered, since a one-sided hinge provides a greater comfort than a double-sided hinge, but a double-sided hinge has a better structural integrity.

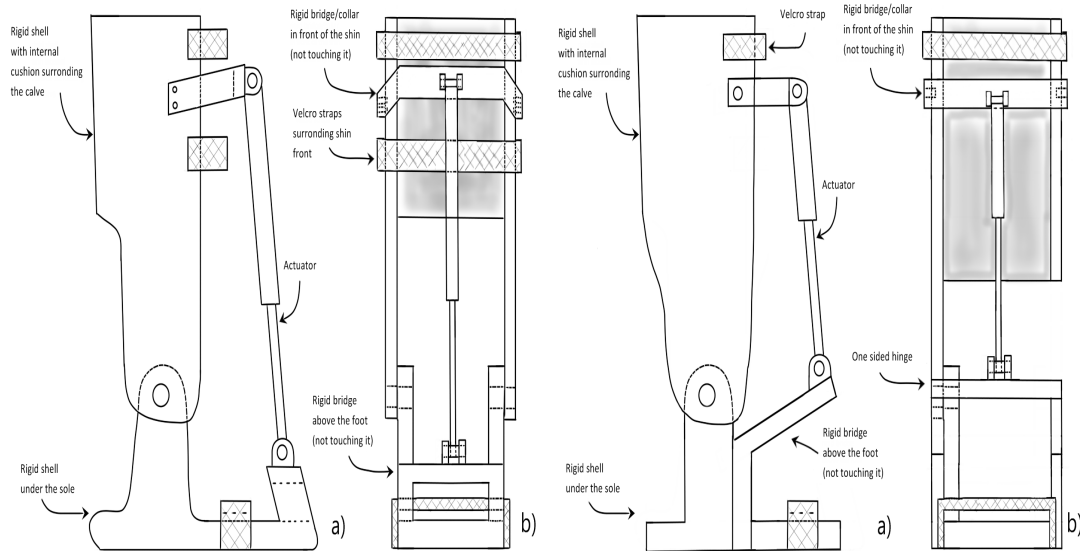
With the previously mentioned ideal solutions in mind the orthosis designs illustrated in Figure 3.1 were created. After meticulously inspecting all the designs it was decided that the beta and delta (3.1b, 3.1d) designs with a one-sided hinge, would not be used, because the structure is prone to bend to the sides due to the actuation forces. And to prevent this the structure would need to be bigger or uses a stiffer material than the one used in a double-sided hinge, which could result in more weight in the lower leg.

In addition, it was decided that a protection on the front, such as in the designs alpha and beta (3.1a, 3.1b) would not be ideal, as the leg would receive inevitably a considerable amount of pressure that would result in discomfort. Due to the considerations mentioned above the gamma design seen in Figure 3.1c was chosen as the best design to create a physical prototype of the ankle exoskeleton.



(A) Alpha

(B) Beta



(C) Gamma

(D) Delta

FIGURE 3.1: Orthosis designs

3.2 Detailed design

Based on the gamma design structure, the 3D rendered model of the exoskeleton prototype shown in Figure 3.2 was created. In addition, from the same 3D model the individual components technical drawings presented in the Appendix C.3 were generated for its later fabrication.

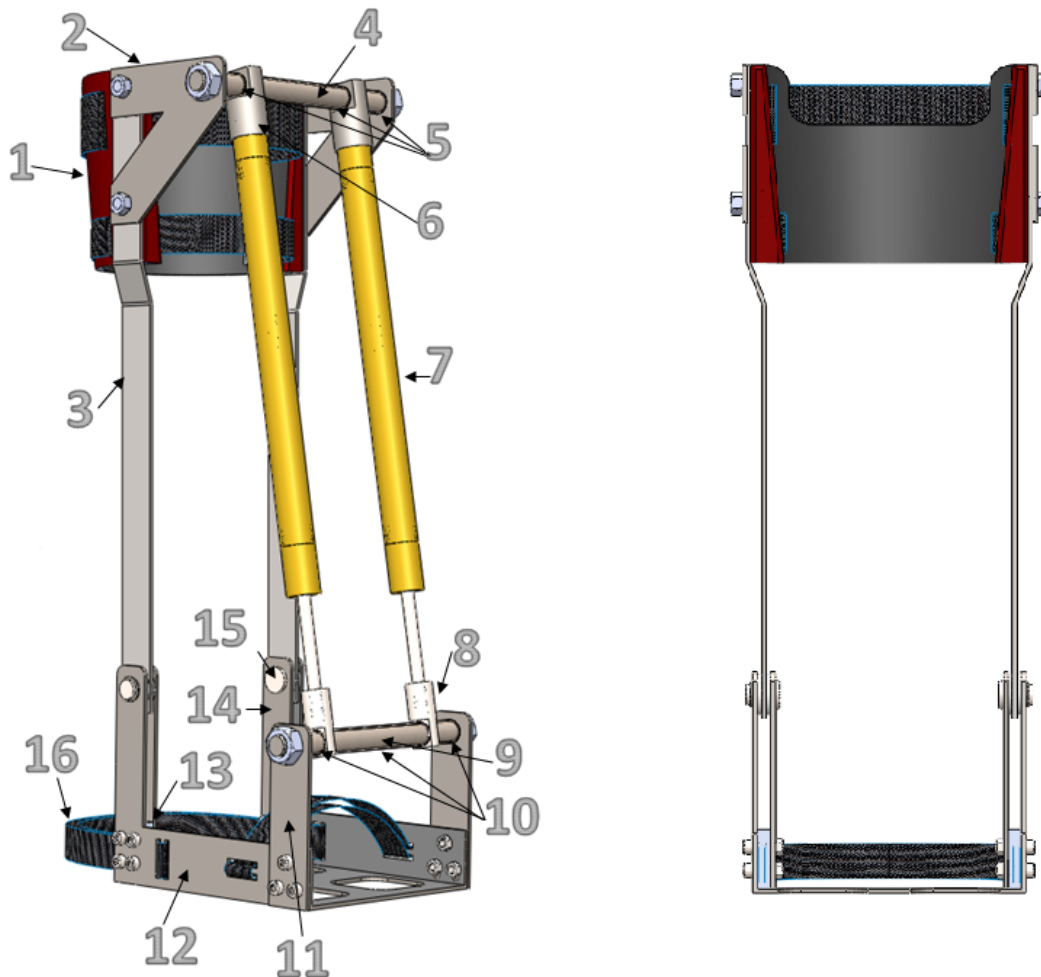


FIGURE 3.2: Isometric view and frontal cross-sectional view of the exoskeleton prototype: 1. Lower leg rest, 2. Shin-hinge frames, 3. Shell-sidebars, 4. Shin-hinge pin, 5. Shin-hinge alignment tubes, 6. Actuator extension cap, 7. Hydraulic actuators, 8. Actuator-rod end, 9. Footplate-hinge pin, 10. Footplate-hinge alignment tubes, 11. Footplate-hinge frames, 12. Footplate, 13. Ankle joint-hinge spacer, 14. Ankle joint hinge internal frames, 15. Ankle joint-hinge precision pin, 16. Velcro straps.

In contrast to the gamma design the final prototype model used a protection shell that only covered the top calf area so that the original lateral sides of the shell could be made of a stronger material and the shell could remain light and elastic to better fit the user's muscles area.

Furthermore, for the shin and foot actuator anchor points instead of using a small hinge and a solid bracelet surrounding the front of the leg, a simpler approach using two metallic plates and a pin to create a hinge were used. This was done because the new approach resulted easier to manufacture and had less theoretical mass than the original concept.

Initially, as in the gamma design, only a single actuator was going to be used in the device, however, after performing a finite element analysis (Appendix C.2) to determine if the hinges would withstand the force requirements for this implementation, it was found that using a single actuator would require a top and low hinge pin of 12 mm of diameter. The problem of using these pins is that they change the dimensions of the final structure in a way that the necessary dorsiflexion range of motion is barely obtained. Hence, two actuators were used to better distribute the actuation force throughout the hinge pins so that a smaller top and bottom hinge pin size could be used.

In addition, the footplate remained almost as the original concept but with the slight difference that now instead of covering the whole foot sole, only the area shown in Figure 3.3 will touch the user's shoe. The reason is that a longer footplate would prevent the toes from bending naturally and that the area covering the heel did not provide any extra advantages.

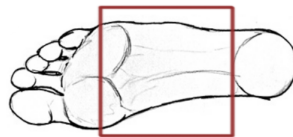


FIGURE 3.3: Footplate covering area.

For the ankle hinge, as seen in the right side of Figure 3.2 the appendix of the footplate hinge and a plate in the internal area of the foot sole were used to create a more stable structure. Lastly, to better fit the exoskeleton to the user's limb, a pair of small slots for the velcro straps were added to the shin shell and foot sole.

Due to time limitations the materials and small components used for the prototype fabrication, were the best available in the University of Twente. Table 3.2 shows the name and material of the components conforming the detailed design shown in Figure 3.2.

TABLE 3.2: Prototype parts list

# of parts	Name	Material	Contribution to the total device weight
1	Shin-shell	Fiberglass/Polyester filler	4.85%
2	Shin-hinge frames	Steel ST37	7.02%
2	Shell-sidebars	Steel ST37	11.55%
1	Shin-hinge pin	Steel ST37	5.1%
6	Actuators alignment tubes	Aluminium	0.49%
2	Actuator extension cap	Steel ST37	5.42%
2	Actuator-rod end	Aluminium	2.64%
1	Footplate-hinge pin	Steel ST37	4.98%
2	Footplate-hinge frames	Steel ST37	3.78%
1	Footplate	Steel ST37	18.11%
2	Ankle joint-hinge spacer	Aluminium	1.01%
2	Ankle joint hinge internal frames	Steel ST37	3.55%
2	Ankle joint-hinge precision pin	Steel ST37	1.15%
2	Hydraulic actuators	Copper	30.35%

4 | Bench test

In this chapter, first, a description of the equipment used to test the performance of the physical prototype is provided. Second, the implemented experiments and their results are discussed. Third, the limitations of the current device and future work are presented. To end the chapter a conclusion of the overall results obtained from the device fabricated in this project is shown.

4.1 Equipment

4.1.1 Testing leg platform

In order to measure the prototype's potential the testing leg presented in Figure 4.1 was used. The testing leg was provided by the BME group and it has four integrated angle sensors located in the hip, knee, ankle, and toes. Furthermore, it also provides two external pressure sensors and a separate loadcell that can be attached to measure tension forces. Force, pressure and angles data are gathered by a Mbed controller and are saved to an SD card.

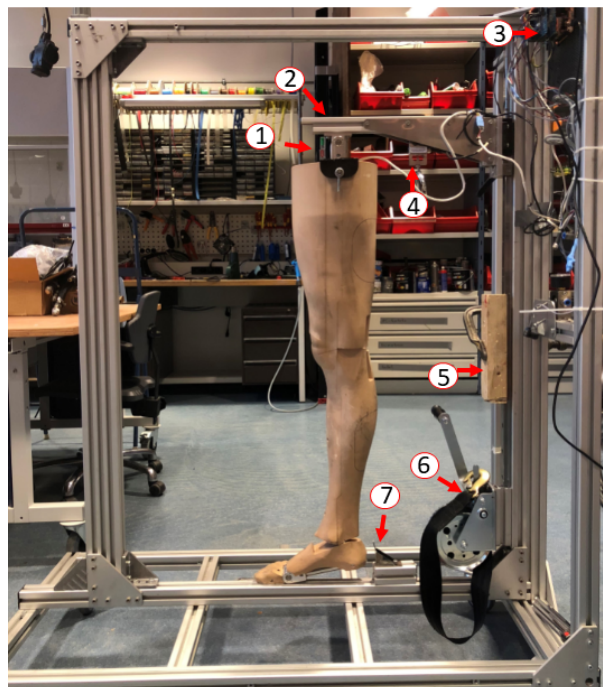


FIGURE 4.1: The illustration of the testing leg platform. 1. Leg upper anchor point, 2. Adjustable frame, 3. Mbed controller, 4. Force loadcell, 5. Adjustable support, 6. Adjustable winch, 7. Heel anchor point

4.1.2 Input stage

The force applied to the exoskeleton hydrostatic cylinders was performed using the input stage provided also by the University of Twente (Figure 4.2). To deliver the force, a single Clippard H9C-6D cylinder (the same model used in the exoskeleton) connected to an electric motor and a mechanical transmission were used. In addition, the input stage control was done using an XPC server and an additional PC running the Matlab/Simulink control script. The force control could be performed using a velocity, voltage and current reference mode. At the moment of the experimentation, the maximum output force that can be obtained from the input stage was 1000 N.

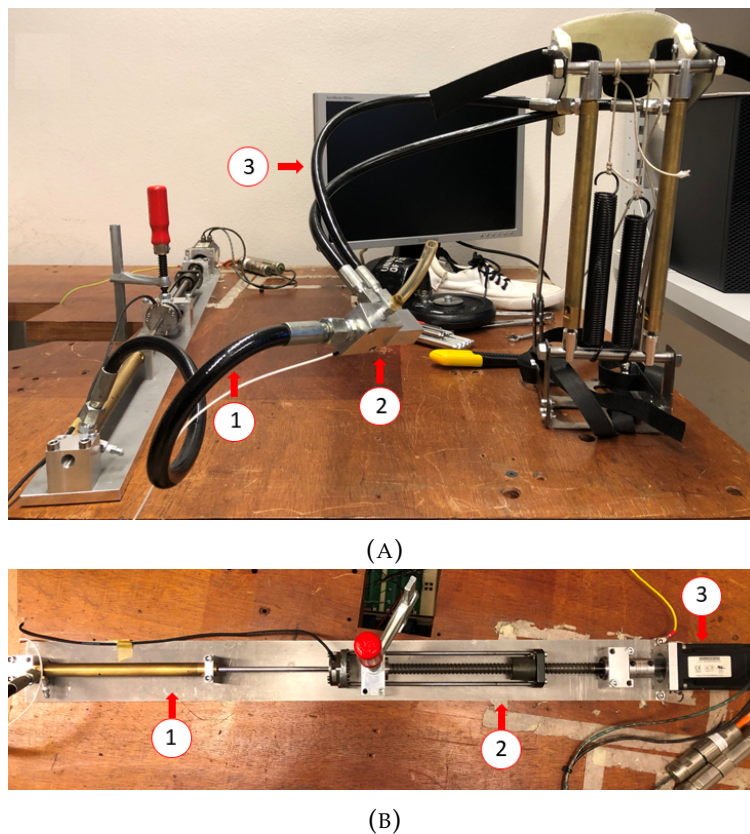


FIGURE 4.2: (A) Frontal and (B) top view of the input stage. A.1. Input stage connector hose, A.2. Flow divider, A.3. Cylinders connector hoses, B.1. Clippard H92C-6D cylinder, B.2. Ballscrew transmission, B.3. Electric servomotor.

4.1.3 Manual pump platform

To determine the maximum ankle torque the device can withstand the test platform presented in Figure 4.3 was created. The platform contains a manual pressure pump with an analog pressure sensor, a depressurizing valve, and a digital loadcell. The pump was filled with the same liquid used in the input stage. The pump pressure sensor can measure up to 100 bar and the loadcell can measure a maximum of 100 Kgf.

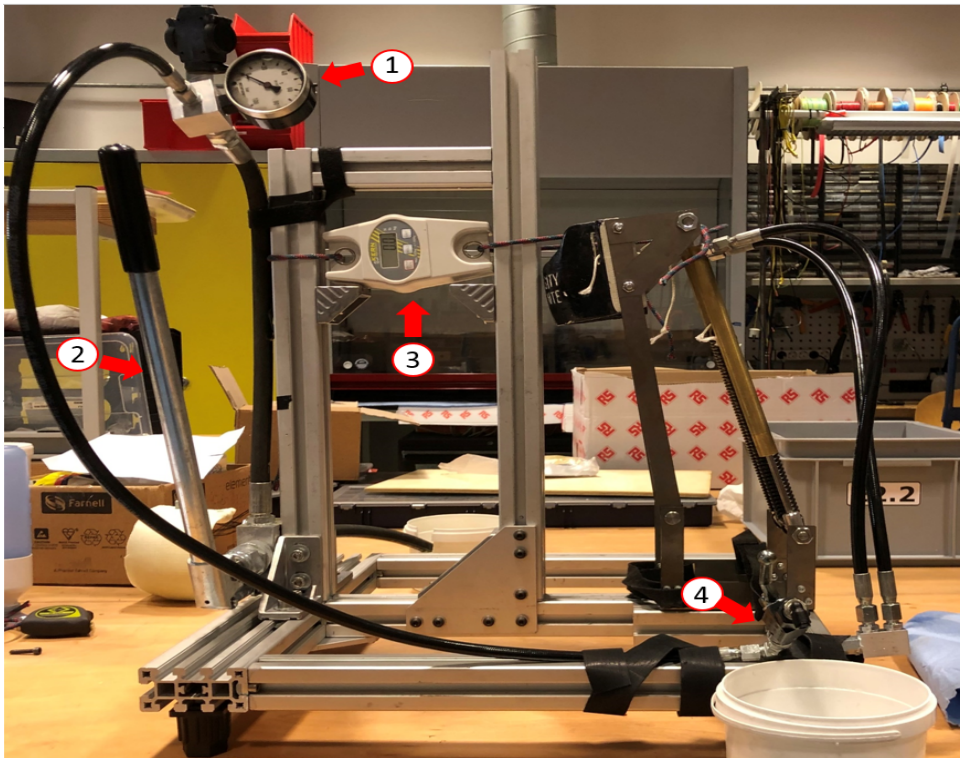


FIGURE 4.3: The illustration of the manual pump testing platform. 1. Analog pressure sensor, 2. Manual pressure pump, 3. Digital loadcell, 4. Depressurizing valve.

4.2 Experiments using the manual pump

For all experiments, the pump was filled with the same liquid solution used in the input stage and the loadcell was connected to the exoskeleton upper pin axis to measure the exoskeleton's reaction force. In addition, the exoskeleton's footplate was fixed using two C-clamps.

Three experiments were performed. In the first, the exoskeleton's back was placed pointing toward the center frame of the testing platform as seen in Figure 4.4a and different pressure values were applied. From each applied pressure the resulting cylinders stroke length was measured and the force value after depressurization was obtained in order to obtain data for the dorsiflexion ankle torque.

For the second, the exoskeleton was rotated 180° so that its front was pointing toward the center frame as seen in Figure 4.4b. As in the first experiment, different pressures were applied and their corresponding resultant cylinder stroke was measured. Unlike the first experiment, the force measurements were done with the cylinders pressurized to obtain the plantarflexion torque. In the last experiment, the exoskeleton was placed as in the second experiment and a stress test was performed. Pressure was applied until the device could not resist more, and the values of the pressure sensor and loadcell just before the exoskeleton bent were noted. Likewise, the resultant cylinder stroke at the bending point was measured so that an approximation of the maximum ankle torque could be calculated.

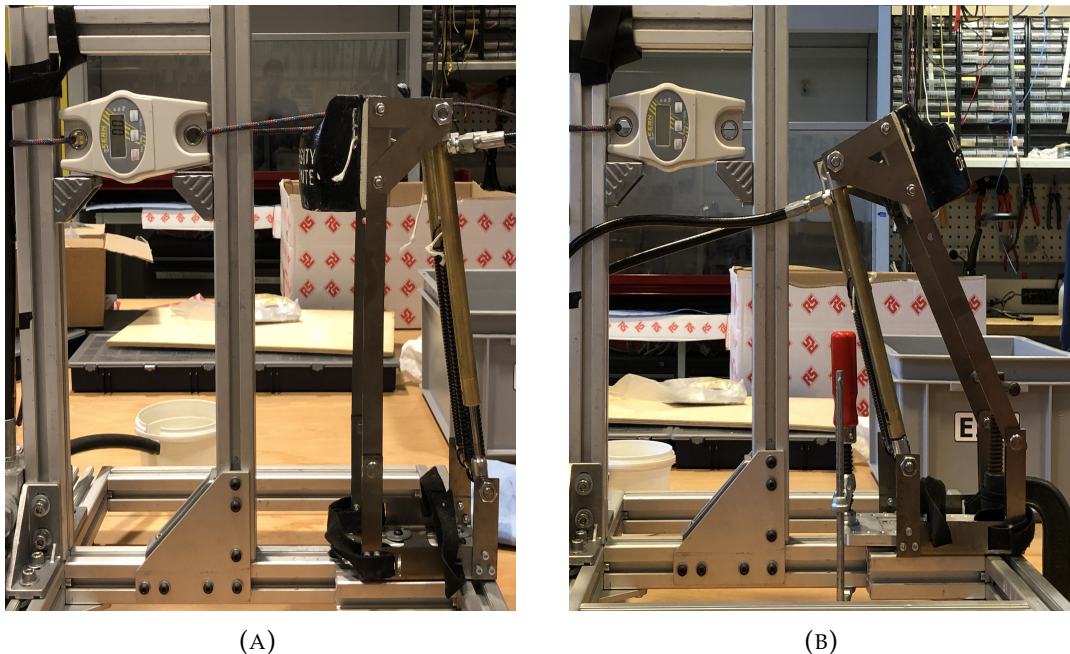


FIGURE 4.4: (A) First manual pump experiment (measurement to determine dorsiflexion torque). (B) Second manual pump experiment (measurement to determine plantarflexion torque).

4.3 Experiments using the testing leg

For the following experiments, a velocity controller was used to manage the force delivered by the input stage. Furthermore, as illustrated in Figure 4.2.A the input stage was connected to both exoskeleton's cylinders. Although delivering an equal force to both exoskeleton's cylinders was not a problem, only a part of the necessary exoskeleton's cylinders stroke could be obtained. The reason is that the total input stage travel is divided into the two exoskeleton's cylinders. As result, only a stroke of 76.2 mm was obtained.

In addition, the exoskeleton was securely attached to the testing leg using the exoskeleton's velcro straps. An additional velcro strap was used around the shoe plate to prevent that the device slipped out since the lifted testing leg's leg's surface had insufficient friction to prevent it from falling.

Originally the exoskeleton was meant to be used wearing a shoe, but for all experiments, no shoe was attached to the testing leg because the dimensions of the foot with the shoe were too big to fit the exoskeleton without touching the foot-hinge pin. Lastly, two springs with a combined spring coefficient of 9.365 kN/m were used as return element to bring the foot back to its maximum dorsiflexion position.

4.3.1 Hanging leg experiment

The goals of this experiment were (1) to measure the available dorsi- and plantarflexion ROM of the exoskeleton, (2) and to test if the device was able to deliver the speed requirements mentioned in Table 1.2. To do so, as shown in Figure 4.5 the testing leg was suspended in the air so that the foot had enough space to move freely.



FIGURE 4.5: Illustration of the hanging leg experiment configuration.

Four trials were performed. In the first trial, the exoskeleton was moved manually from the maximum dorsiflexion position to the maximum plantarflexion position. In the second trial, the exoskeleton was connected to the input stage and a constant 15mm/s velocity value was used as the control reference to again move the foot from the maximum allowed dorsiflexion angle as seen in Figure 4.5 to the maximum plantarflexion angle allowed by the input stage. Finally, in the third and fourth trial, the same procedure was done but using a constant velocity value of 150 mm/s and 480 mm/s (maximum input stage speed) respectively.

4.3.2 Stepping leg experiment

Since the testing leg plus the upper frame has a weight of 13.3 kg which is about the average leg weight of an 80kg person [19], it was thought that performing an experiment in which the exoskeleton lifted the testing leg from the ground would give a good insight of the force that the device needs to assist a real subject. Hence, The goal of this experiment was to measure the force necessary to lift the weight of the testing leg from the ground. This was done using the loadcell attached to the input stage cylinder. The reason the loadcell of the testing leg was not used is that in order to take a force measurement the frame where the upper anchor point of the leg is attached would need to be fixed, however, if this was done there was the risk of damaging the leg. For that reason, in the experiment, the top frame was not fixed.

To do so, as seen in Figure 4.6, the leg was completely extended, the foot was located flat to the bench test ground and the knee joint was locked. This was done because the additional friction necessary to extend the knee, in the bent leg configuration generates an initial huge force spike. Hence, the measurements would not represent the real force necessary to lift only the leg weight.



FIGURE 4.6: Illustration of the stepping leg experiment.

4.4 Results

4.4.1 Range of motion

Table 4.1 presents a summary of the maximum angles from the datasets presented in Figures 4.7 and 4.8. The maximum dorsiflexion angle obtained in the active trials (Figure 4.8c) was of 21.25° , while the maximum plantarflexion angle was of 12.50° . Both maximum dorsiflexion and plantarflexion angles in all active trials are significantly lower than the values obtained in the manual test (figure 4.7). In the manual test a total ROM of almost 50° was obtained, of which 24.42° were of dorsiflexion and 25.51° of plantarflexion.

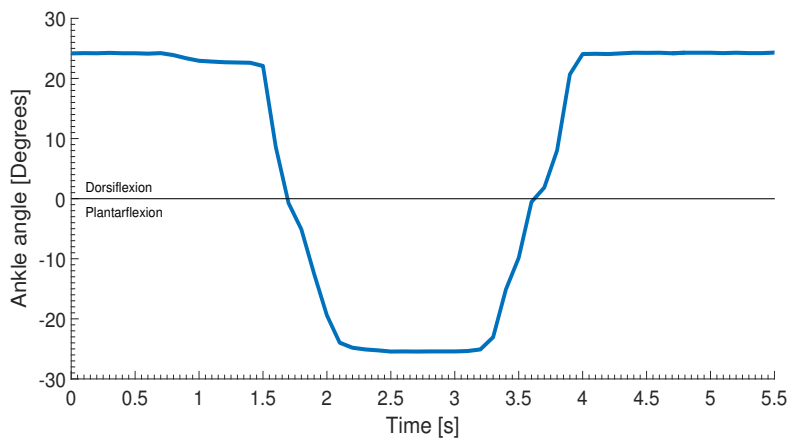
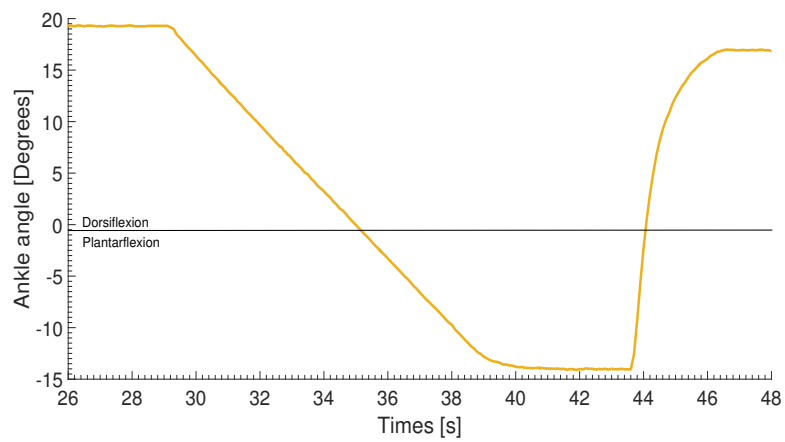


FIGURE 4.7: Exoskeleton's ROM in the manual trial

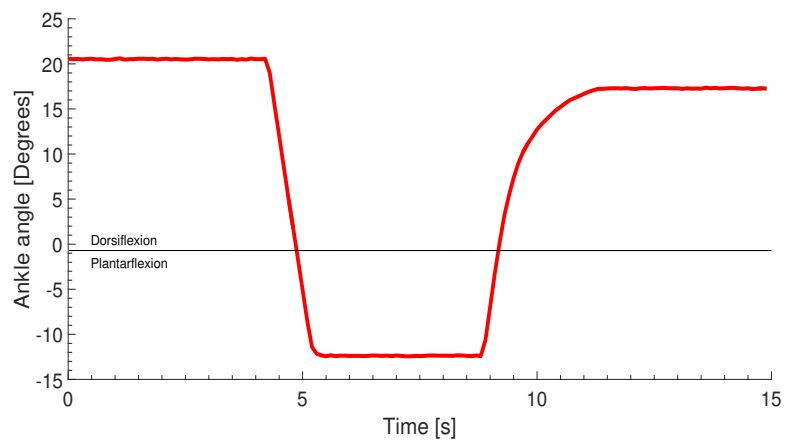
TABLE 4.1: ROM results of the "hanging leg" experiment

Velocity reference	Max. Dorsiflexion	Max. Plantarflexion
15 mm/s	19.38°	14.10°
150 mm/s	20.61°	12.44°
480 mm/s	21.25°	12.50°
-*	24.41°	25.51°

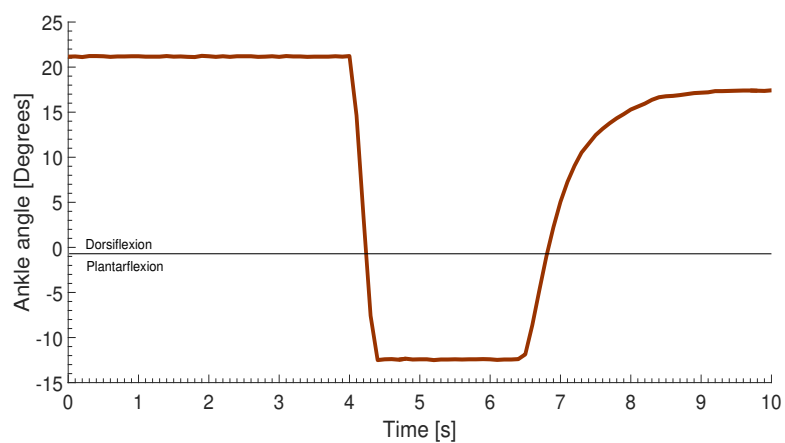
*Manual trial



(A)



(B)



(C)

FIGURE 4.8: Exoskeleton's active trials using a control velocity reference of A) 15 mm/s, B) 150 mm/s, C) 480 mm/s.

4.4.2 Exoskeleton's cylinder velocity

In order to obtain an estimate of the maximum angular velocity at which the cylinders could work, a trial using the maximum velocity reference control of the input stage was done. From this trial the ROM data presented in Figure 4.8c were obtained. These data was differentiated with respect time and the dataset presented in Figure 4.9 was obtained. It was found that the maximum ankle angular velocity for this trial was 113.16 deg/s. This value belongs to the phase in which the cylinders are extended to reach the maximum testing leg's foot plantarflexion angle.

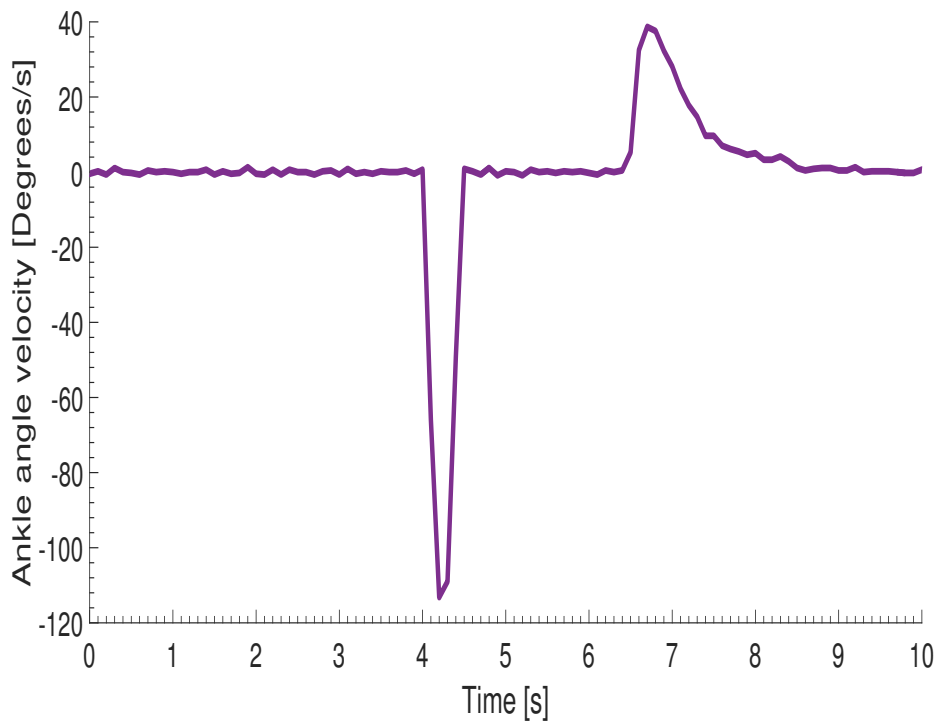


FIGURE 4.9: Ankle angular velocity obtained from the ROM dataset of the 480 mm/s velocity control reference trial

4.4.3 Forces

Although it was observed that the device was successfully capable of lifting the testing leg, due to hardware limitations it was not possible to record data to determine the exact force the cylinders delivered. However, as illustrated in Figure 4.10 it was found that the necessary input stage force to lift the testing leg is 255 N. Assuming there are no energy losses in the system the exoskeleton's cylinders combined force should have been 500 N.

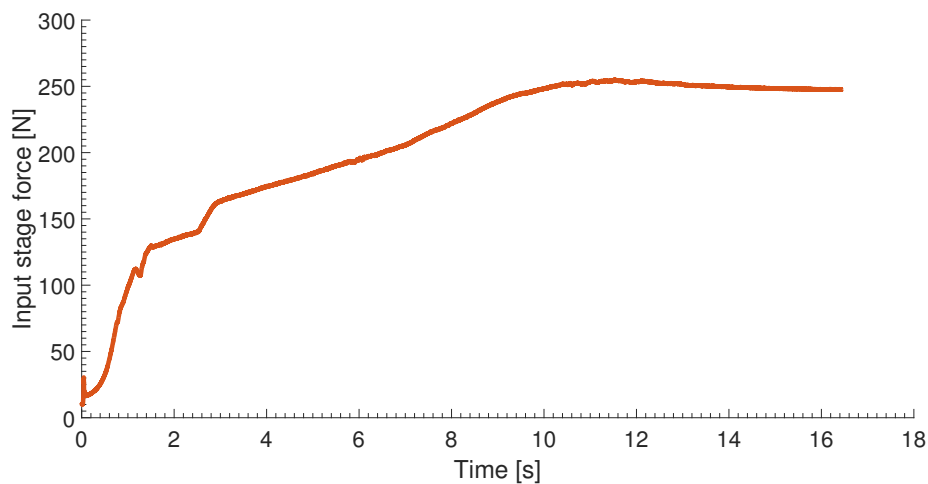


FIGURE 4.10: Input stage force data of the stepping leg experiment using a velocity reference of 15 mm/s

Ankle torque

The approximate ankle torque T_a was calculated using equation 4.1. From which the moment arm r was obtained using trigonometry and the cylinder stroke measurement data from the manual pump experiments (Appendix D, Table D.1). Likewise, The force F is the loadcell data in Newtons from the same experiment. The obtained torque values are presented in Figure 4.11. This values are an approximation due to the uncertainty of the force data and the approximation of the moment arm.

$$T_a = r * F \quad (4.1)$$

During the stress test, a gradual pressure was applied until the exoskeleton reached its limit. As seen in Figure 4.12, the parts that deformed were the right sidebar and the right lower pin plate from the footplate. Just before the structure failed a pressure of 80 bar and a force of 38.2 kgf were observed. Using this values it is estimated that the maximum ankle torque that the structure could withstand was of 115.9 Nm (Plantarflexion).

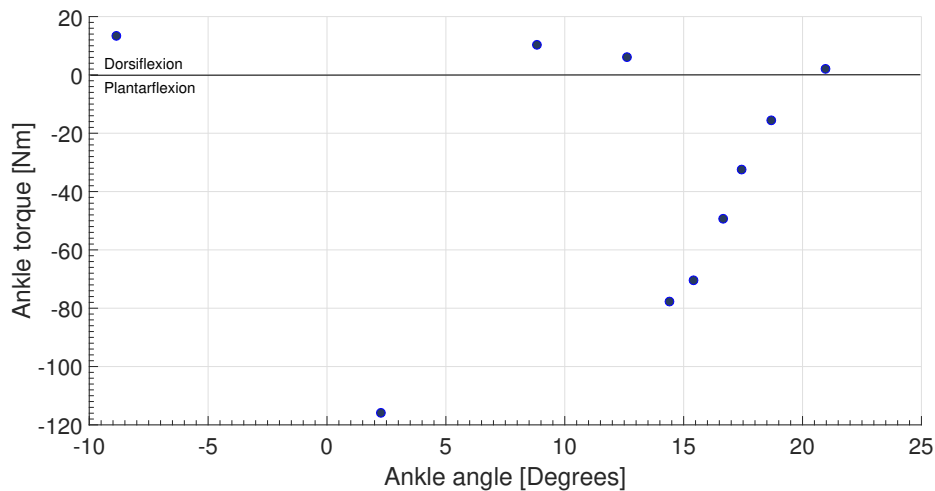


FIGURE 4.11: Ankle torque results of the manual pump test plotted against the ankle angle at which each measurement was taken.



(A)



(B)

FIGURE 4.12: (A) Back and (B) front view of the exoskeleton after the stress test.

4.4.4 Results vs requirements

In order to summarize and grade the overall performance of the developed device, Table 4.2 was generated.

TABLE 4.2: Results and requirements comparison

Description	Required	Obtained	Goal grade
Exoskeleton ROM	Total ROM: 55° PF: 35° DF: 20°	Total ROM: 80.41° PF: 56° DF: 24.41°	A
Exoskeleton weight	Max : 1.5 kg	2.2 kg	NA
Min. actuation torque for climbing, walking and STS motion	Min. walking plantarflexion torque: 165 Nm, Min. walking dorsiflexion torque: 24 Nm Min. stairs climbing plantarflexion: 132 Nm Min. stairs climbing dorsiflexion: 3.2 Nm Min. STS plantarflexion: - Min. STS dorsiflexion: 67 Nm	Max. recorded PF torque: 115.9 Nm Max. recorded DF torque: 4.87 Nm	NA
Stairs dimensions in which the device needs to function	Stair riser dimension: 0.102-0.178 m Min stair tread depth: 0.279 m	-	A
Max. area dimensions for the orthosis design	Total height: 0.51 m (from the foot sole to the knee) Anterior leg space: 0.26 - 0.286 m (42 - 45 EU shoe size) Posterior leg space: 0.16 m (arbitrarily selected) External leg space: no specific limit. Max internal leg space: 0.20 m	Total height: 0.425 m Anterior leg space: 0.13 m Posterior leg space: 0 External leg space: 0.03 m Max internal leg space: 0.02 m	A
Pressure limits for different lower leg areas	Max. posterior lower leg PPT (Pain Pressure Threshold): 545 KPa Max. anterior lower leg PPT: 416 KPa Max. foot dorsum PPT : 360 KPa Max. foot sole PPT: 240 KPa	/	-
Min. actuation speed for climbing, walking and STS motion	Min. walking plantarflexion angular velocity in the ankle joint: 150 deg/s Min. walking dorsiflexion angular velocity in the ankle joint: 55 deg/s Min. stair climbing plantarflexion angular velocity in the ankle joint: 60 deg/s Min. stair climbing dorsiflexion angular velocity in the ankle joint: 61.7 deg/s Min. STS plantarflexion angular velocity in the ankle joint: 20 deg/s Min. STS dorsiflexion angular velocity in the ankle joint: 25 deg/s	Max. recorded PF angular velocity: 113.16 deg/s Max. recorded DF angular velocity: 38.67 deg/s	PA
Total DOF	1 (sagittal plane)	1(sagittal plane)	A

A = Achieved, NA = Not achieved, PA = Possibly achieved, / = Not obtained, PF = Plantarflexion, DF = Dorsiflexion - = not applicable

5 | Discussion

This chapter starts with a more in-depth discussion about the results obtained during this project. Later, the limitations that affected the final experiment results are mentioned and it finalizes giving some recommendations to improve the future design of the ankle exoskeleton.

5.1 Interpretation of results

5.1.1 Range of motion

The reason the initial dorsiflexion angles in the active trials are lower than in the manual trial is that the exoskeleton slid down from the leg. The testing leg did not provide enough friction so that the calf shell stayed in position and because of that a small gap between the foot plate and the foot occurred, that as a result reduced the measured dorsiflexion angle. Additionally, it is suspected that the reason the end dorsiflexion angle do not return to its original position is that the return elements got slightly loose when the exoskeleton was collocated on the leg and that there was still a significant amount of air in the hydraulic system. In addition, the great reduction in plantarflexion in the active trials was not due to the exoskeleton play, but from the limitations of the input stage, as only 76.2 mm of the 120 mm necessary for the actuator stroke could be delivered.

From all trials, the greatest ROM was recorded in the manual trial. In one hand the maximum Plantarflexion ROM recorded in this trial was of 25.51° , however, this value does not represent the maximum plantarflexion angle that the device can deliver but as illustrated in Figure D.3 in Appendix D, it is the maximum range that the testing leg's foot can get. The real maximum plantarflexion angle that the device can reach is approximately 56° . Which is, as shown in Figure D.2, more than necessary to cover the natural ROM of the foot.

On the other hand, the maximum recorded dorsiflexion angle is indeed the real physical limit of the exoskeleton. This value is in accordance with the theoretical angle obtained from the CAD model. Hence, it can be assured that the real maximum dorsiflexion angle is indeed the value recorded in the manual trial. After discussing the different results presented in Table 4.1, it can be concluded that the device is capable of delivering the ROM requirements of this project.

5.1.2 Exoskeleton's cylinder velocity

Since it was not possible to use a higher velocity control reference with the input stage, it could not be proved if the device was able to deliver the minimum plantarflexion requirements for walking. However, with the results obtained it can be assured that the device can deliver at least the minimum plantarflexion requirements to climb stairs and to perform an STS motion.

Judging by the maximum dorsiflexion angular velocity value obtained in the hanging leg experiments, it seems that the springs only provide enough assistance to reach the minimum STS dorsiflexion angular velocity requirements. However, this may not be the case, since more than likely a lower velocity was obtained due to the return elements working against the gravity as the exoskeleton was hanging in the air. It is expected that when the exoskeleton is worn, the gravity now working in favor of the return element will generate enough dorsiflexion angular velocity to reach the minimum requirements of waking and stair climbing.

5.1.3 Forces

Due to a bad sampling of the angular motion data on the stepping leg experiments, it was not possible to get enough information to determine the ankle torque occurring throughout the whole experiment. Furthermore, since the available equipment was not suitable to obtain an accurate measure of the force occurring in the cylinders only the input stage force data was obtained. As previously mentioned in the results, the maximum recorded input stage force was 255 N. To make an approximation of the total maximum force that the exoskeleton delivered it is assumed that there was no energy losses in the system. Considering that two cylinders were used as the exoskeleton actuation method, this would mean that ideally the total maximum force that the exoskeleton delivered was 500 N. Using the D.A. Winter [18] ankle torque and angle dataset, it is known that the maximum force that the exoskeleton needs to withstand to assist gait is 1300 N. This means that ideally, the exoskeleton provided 38% of the maximum force the exoskeleton is expected to withstand.

As illustrated in 4.2 the maximum plantar and dorsiflexion torques found in the manual pump experiments are not sufficient to assist any of the gait requirements discussed in this project. It was already expected that by using a passive return to assist dorsiflexion the dorsiflexion ankle torque requirements would not be reached. However, it was surprising that also the plantarflexion ankle torque requirements for all human movements were not reached. It is clear that the device still lacks structural stability in order to withstand greater ankle torques. However, since a 70% of the maximum ankle torque magnitude in the requirements (165 Nm in walking plantarflexion) was obtained, it is expected that with some slight changes to the lateral frames of the device, all ankle torque requirements of this project will be achieved.

5.2 Limitations

During the fabrication process, the greatest limitation was the restriction of time. For example, to save time the cylinders used in the exoskeleton were chosen from the best option of those that have already been used with the hydrostatic input stage. Because of that, the size of the cylinder was not the best size that could have been used. As a result the final prototype dimensions, although inside the requirements limitations, were bigger still considerably big.

Similarly, another affected factor was the prototype's weight. In the end, the weight requirements were not achieved, because the material used to fabricate the parts was not selected to obtain an optimal weight but from the availability of materials at the University of Twente.

In the case of the prototype testing, the greatest limitation was the equipment used in the experiments. For example, the testing leg is not specifically designed to test an exoskeleton such as the one presented in this project. As a result, the original exoskeleton shell (black shell, Figure D.2) could not be used and instead a custom made shell (white shell, Figure D.3) with the dimensions of the testing leg calf was needed. Moreover, since the available load cell in the testing leg is not designed to obtain either a direct force measure from the exoskeleton cylinders nor the force being applied in the leg it could not be used to obtain accurate force measures.

Aside from that, the input stage is not able to deliver the speed and cylinder stroke desired for this implementation. This is the reason that (1) in the active test of the hanging leg experiment only a part of the maximum plantarflexion is observed and (2) it was not possible to confirm if the exoskeleton cylinders would be able to reach the minimum speed requirements for gait.

Lastly, the exoskeleton structure was not very ergonomic, because to wear it, first the user would need to take his shoe off, then, secure the shoe in the exoskeleton's footplate and later slide its leg from the top of the exoskeleton to finally put the shoe again and secure the exoskeleton's calf protection to its leg. Moreover another aspect that reduced the user comfort perception when the device was worn was that the device only had a single DOF. Especially for stair climbing as found in [20], it was really notable that the motion in the transverse plane (Ankle's internal and external rotation) was necessary, as there was a certain discomfort in each ascending step and when rotating to start descending. Apart from that in order to fit different lower leg limbs sizes as occurred with the testing leg, it is necessary to create a custom-made calf protection, which at the end is not an ideal solution.

5.3 Recommendations

For future work, it is highly recommended to implement an extra DOF for internal/external rotation. Since as it was observed, having motion solely in the sagittal plane does not allow to perform a natural movement of the lower limb as it highly reduces the user comfort.

Aside from that, it is also recommended to investigate for smaller and powerful hydraulic actuators that can be used in a similar configuration. Since one point that was observed in the design phase is that in contrast to the plantarflexion ROM that can be easily increased using a longer stroke, the dorsiflexion ROM is mainly limited by the position and the length of the user actuator.

In addition, it is important to develop a device that is easier to wear. Because even if in this project this does not limit the operation of the device, it does affect the user experience, without mentioning it makes the experimentation preparation tasks harder than they should. One way to that would be to consider a flexible calf protection made of a textile material since in reality, the sole function of the calf protection was to keep the device in place and not to withstand a force. Moreover, considerations need to be taken for the lateral bar conforming the exoskeleton, as it can be seen in Figure 4.12 from the stress test, these parts were the main factor that compromised the exoskeleton's structural integrity.

In the case of materials, although steel is very strong and it is easy to work with, it does add a considerable amount of weight to the design. Hence, future work should also be a focus in investigating alternative materials that are light but strong so that the total mass of the device can be reduced.

Lastly, preparing a custom-made bench test to fully measure the potential of the device should be one of the main tasks to do. Since, as mentioned in the discussion section, adapting to an already made bench test can heavily affect the end results of the tested device.

6 | Conclusion

Ankle-foot orthoses are great assistive tools for people suffering from lower limb muscle weakness, however, they still have a long way to be comfortable and optimal functional devices. As seen in this project, generating a new device that is capable of meeting the minimum requirements needed to perform the basic human movements is not an easy task. Many factors such as the device weight, actuation method and power source can significantly affect the performance of such devices.

The device created in this project proved to be a promising approach as a solution to the development of an ankle-foot orthosis. For example, it provided the greatest ROM of all the compact devices introduced in the state of the art. In addition, its design allowed it to perform different human movements such as walking, stair climbing and STS transfer without having any collision with its surrounding environment. Furthermore, even when the ankle angular velocity requirements of this project were not obtained the exoskeleton's electro-hydrostatic actuation still could generate an ankle angular velocity of 113.16 deg/s, which represent a 75% of the total maximum ankle angular velocity found in gait. Aside from that, it was able to generate a 70% of the total maximum ankle torque of walking. Which was only because of the structural limitations of the exoskeleton and not by the capacity of the electro-hydrostatic actuation. Because of that, it is concluded that an electro-hydrostatic actuation is a valuable alternative actuation method for Ankle-foot orthoses.

Nonetheless, hydraulic based actuation methods still present significant limitation that needs to be taken in to account. For example, the cylinder's size. Most of the hydraulic cylinders found in the market are too large to be used in ankle-foot orthoses. As a result, even when the smaller commercial size is used it can greatly increase the size of the final device just as in this project. A solution for that is to use custom made cylinders, however, if they are used, it is necessary to consider that the maximum power of the actuator is limited to its size. Another factor to consider is its dependency on a hydraulic power source. Although a portable power source for an ankle-foot orthosis has been already developed, there is not yet a portable and compact hydraulic source that is powerful enough to provide the minimum torque requirements of human gait[12].

As has been illustrated in this project, there is not yet a device that is fully capable of optimally support the most basic human movements. And looking to the current world health trends, it is estimated that 38% of the world adult population will suffer from obesity, which means many of them would be in high risk of suffering a stroke, that could result in additional motion impediments [21]. Hence, it is urgent that more research is done to find better solutions for lower limb assistive and rehabilitation devices.

Acknowledgements

First of all, I would like to thank Professor Herman van der Kooij and all the people from the Biomechanical Engineering department, for allowing me to be part of this project and their support. In special I would like to thank my daily supervisors Dr. Allan Veale, Ir. Kyrian Staman and Ir. Martijn Grootens. I'm so grateful for your patience and support through all the project, but overall I'm grateful because I was able to learn a lot from each of you.

Also, I would like to dedicate some words to Ing. Quint Meinders and Ing. Wouter Abbas. They helped me through the fabrication of the exoskeleton prototype and served as mentors to define the final design. Despite their busy schedule, they always found the time and were eager to help me, which is something I will always remember.

Aside from that, I would like to thanks my friends of the not so secret, "secret coffee society". Ewoud, Tom, Paul, Justin you made my days at the office more enjoyable and always reminded me that to improve you also need to take some rest to think properly.

In the same way, I would like to thank my multicultural family, for the laughs, shared times and experiences that made me feel I had a second home in the Netherlands. Aggelos, Alessio, Aina, Ainhoa, Ander, Bea, Celia, Dadi, Erick, Helena, Irene, Jaime, Julia, Laura, Maria, Ranli, Richella, Niki and Niko. Even if you did not realize it, every single of you have a special place in my heart, in a way or another, you molded the person I am today and for that, I will always be in debt to you.

Especially, I'm deeply grateful to Martin Carrasco, Pablo Cop and Tarek Gethe. These three wonderful persons were my loyal friends (almost like brothers) and roommates throughout all my masters. There are no words that can express how fortunate I feel to have ever met you and I hope I will continue seeing you in the future.

Lastly but not least, I would like to thank my parents and family. Because without them I would not have been here in the first place. You always supported me and never not even for a second doubted. I hope one day I can return everything you have done for me.

Bibliography

- [1] K. Z. Takahashi, M. D. Lewek, and G. S. Sawicki, "A neuromechanics-based powered ankle exoskeleton to assist walking post-stroke: A feasibility study," *Journal of Neuroengineering and Rehabilitation*, vol. 12, no. 1, pp. 1–13, 2015.
- [2] Y. Bai, X. Gao, J. Zhao, F. Jin, F. Dai, and Y. Lv, "A portable ankle-foot rehabilitation orthosis powered by electric motor," *The Open Mechanical Engineering Journal*, vol. 9, no. 1, pp. 982–991, 2015. [Online]. Available: <http://benthamopen.com/ABSTRACT/TOMEJ-9-982>
- [3] Y. L. Park, B. R. Chen, N. O. Pérez-Arancibia, D. Young, L. Stirling, R. J. Wood, E. C. Goldfield, and R. Nagpal, "Design and control of a bio-inspired soft wearable robotic device for ankle-foot rehabilitation," *Bioinspiration and Biomimetics*, vol. 9, no. 1, 2014.
- [4] n.a., "Facts and figures about stroke," World Stroke Organization, n.d. [Online]. Available: <https://www.world-stroke.org/component/content/article/16-forpatients/84-facts-and-figures-about-stroke>
- [5] N. Alexander, G. Strutzenberger, L. M. Ameshofer, and H. Schwameder, "Lower limb joint work and joint work contribution during downhill and uphill walking at different inclinations," *Journal of Biomechanics*, vol. 61, pp. 75–80, 2017. [Online]. Available: <http://dx.doi.org/10.1016/j.jbiomech.2017.07.001>
- [6] T.-w. P. Huang and A. D. Kuo, "Mechanics and energetics of load carriage during human walking," *Journal of Experimental Biology*, vol. 217, no. 4, pp. 605–613, 2014. [Online]. Available: <http://jeb.biologists.org/cgi/doi/10.1242/jeb.091587>
- [7] S. Galle, P. Malcolm, S. H. Collins, and D. De Clercq, "Reducing the metabolic cost of walking with an ankle exoskeleton: interaction between actuation timing and power," *Journal of Neuroengineering and Rehabilitation*, vol. 14, no. 1, pp. 1–16, 2017.
- [8] A. H. Weerasingha, W. P. K. Withanage, A. D. K. H. Praganathikala, R. K. P. S. Ranaweera, and R. A. R. C. Gopura, "Powered ankle exoskeletons : existent designs and control systems," *The 2018 International Conference on Artificial Life and Robotics*, pp. 76–83, 2018.
- [9] K. Staman, A. J. Veale, and H. V. D. Kooij, "The PREHydrA : a passive return , high force density , electro-hydrostatic actuator concept for wearable robotics," pp. 1–6.
- [10] Z. Wang and E. T. Hsiao-Weckslar, "Design of a compact high-torque actuation system for portable powered ankle-foot orthosis," *Journal of Medical Devices*, vol. 10, no. 3, 2016.

- [11] A. B. Zoss, H. Kazerooni, and A. Chu, "Biomechanical design of the berkeley lower extremity exoskeleton (BLEEX)," *IEEE/ASME Transactions on Mechatronics*, vol. 11, no. 2, pp. 128–138, 2006.
- [12] M. Noël, B. Cantin, S. Lambert, C. M. Gosselin, and L. J. Bouyer, "An electrohydraulic actuated ankle foot orthosis to generate force fields and to test proprioceptive reflexes during human walking," *IEEE Transactions on Neural Systems and Rehabilitation Engineering*, vol. 16, no. 4, pp. 390–399, 2008.
- [13] B. Neubauer and W. Durfee, "Preliminary design and engineering evaluation of a hydraulic ankle-foot orthosis," *Journal of Medical Devices*, vol. 10, no. 4, 2016. [Online]. Available: <http://medicaldevices.asmedigitalcollection.asme.org/article.aspx?doi=10.1115/1.4033327>
- [14] L. M. Mooney, E. J. Rouse, and H. M. Herr, "Autonomous exoskeleton reduces metabolic cost of human walking during load carriage," vol. 11, no. 1, pp. 1–5, 2014.
- [15] C. Meijneke, W. van Dijk, and H. van der Kooij, "Achilles: an autonomous lightweight ankle exoskeleton to provide push-off power," *IEEE RAS/EMBS International Conference on Biomedical Robotics and Biomechatronics*, pp. 918–923, 2014. [Online]. Available: <http://ieeexplore.ieee.org/lpdocs/epic03/wrapper.htm?arnumber=6913898>
- [16] W. Van Dijk, C. Meijneke, and H. Van Der Kooij, "Evaluation of the achilles ankle exoskeleton," *IEEE Transactions on Neural Systems and Rehabilitation Engineering*, vol. 25, no. 2, pp. 151–160, 2017.
- [17] K. A. Witte, J. Zhang, R. W. Jackson, and S. H. Collins, "Design of two lightweight, high-bandwidth torque-controlled ankle exoskeletons," *IEEE International Conference on Robotics and Automation*, pp. 1223–1228, 2015.
- [18] D. A. Winter, "The biomechanics and motor control of human gait", 2nd ed. Waterloo, Ontario, CA: (n.p.), 1987.
- [19] J. Hamill and K. M. Knutzen, "Biomechanical Basis of Human Movement," 2013.
- [20] H.-C. LIN, T.-W. LU, and H.-C. HSU, "Three-Dimensional analysis of kinematic and kinetic coordination of the lower limb joints during stair ascent and descent," vol. 16, no. 2, pp. 101–108, 2004. [Online]. Available: <http://www.worldscientific.com/doi/abs/10.4015/S1016237204000153>
- [21] A. Hruby and F. B. Hu, "The Epidemiology of Obesity: A Big Picture," *Pharmacoeconomics*, vol. 33, no. 7, pp. 673–689, 2015.
- [22] K. H. Cho, Y. Jeon, and H. Lee, "Range of motion of the ankle according to pushing force, gender and knee position," *Annals of Rehabilitation Medicine*, vol. 40, no. 2, pp. 271–278, 2016.
- [23] A. Protopapadaki, W. I. Drechsler, M. C. Cramp, F. J. Coutts, and O. M. Scott, "Hip, knee, ankle kinematics and kinetics during stair ascent and descent in healthy young individuals," *Clinical Biomechanics*, vol. 22, no. 2, pp. 203–210, 2007.

- [24] M. K. Mak, O. Levin, J. Mizrahi, and C. W. Hui-Chan, "Joint torques during sit-to-stand in healthy subjects and people with parkinson's disease," *Clinical Biomechanics*, vol. 18, no. 3, pp. 197–206, 2003.
- [25] R. L. Waters and S. Mulroy, "The energy expenditure of normal and pathologic gait," *Gait and Posture*, vol. 9, no. 3, pp. 207–231, 1999.
- [26] H. P. Crowell III, A. C. Boynton, and M. Mungiole, "Exoskeleton power and torque requirements based on human biomechanics," 2002.
- [27] C. L. Brockett and G. J. Chapman, "Biomechanics of the ankle," *Orthopaedics and Trauma*, vol. 30, no. 3, pp. 232–238, 2016. [Online]. Available: <http://dx.doi.org/10.1016/j.mporth.2016.04.015>
- [28] S. Vallabhajosula, C. W. Tan, M. Mukherjee, A. J. Davidson, and N. Stergiou, "Biomechanical analyses of stair-climbing while dual-tasking," vol. 48, no. 6, pp. 921–929, 2015.
- [29] International building code for stair treads and risers. [Online]. Available: <http://www.centurygrp.com/Images/Interior/stair%20treads/internationalbuildingcodestairtreadsrisers.pdf>
- [30] Overview of the international building code. [Online]. Available: <https://www.iccsafe.org/codes-tech-support/codes/2018-i-codes/ibc/>
- [31] R. Kirby, N. Price, and D. Macleod, "The Influence of foot position balance on standing," *Journal of Biomechanics*, vol. 20, pp. 423–427, 1987.
- [32] J. C. Moreno, F. J. Brunetti, J. L. Pons, J. M. Baydal, and R. Barberà, "Rationale for multiple compensation of muscle weakness walking with a wearable robotic orthosis," *IEEE International Conference on Robotics and Automation*, no. April, pp. 1914–1919, 2005.
- [33] S. Xiong, R. S. Goonetilleke, and Z. Jiang, "Pressure thresholds of the human foot: measurement reliability and effects of stimulus characteristics," *Ergonomics*, vol. 54, no. 3, pp. 282–293, 2011.
- [34] L. S. Adiputra, S. Parasuraman, M. K. Khan, and I. Elamvazuthi, "Bio mechanics of Desending and Ascending Walk," *Procedia Computer Science*, vol. 76, pp. 264–269, 2015.
- [35] M. E. Roebroek, C. A. Doorenbosch, J. Harlaar, R. Jacobs, and G. J. Lankhorst, "Biomechanics and muscular activity during sit-to-stand transfer," *Clinical Biomechanics*, vol. 9, no. 4, pp. 235–244, 1994.

A | Requirements notes

Appendix A presents the background research and reasoning to determine the requirements for the fabrication of this project's ankle exoskeleton. Each section in this chapter correspond to one of the individual parameters presented in Table 1.2.

A.1 Range of motion

To determine the necessary ROM, the full foot ROM in walking, STS motion, upward and downward stair climbing were investigated. First, the whole ROM of the foot was obtained from the study of K. H. Cho et al. [22]. In this study, different pressure forces were applied to the foot of a subject, and the observed ankle ROM was measured. For a neutral leg position (straight) the average natural maximum plantar and dorsiflexion angles (range without applying an external force) were of 40° and 22° respectively.

Second, the ascending and descending stair ROM was found in the study by A. Protopapadaki et al. [23]. To determine the ROM they used the kinematic data of eleven subjects when descending and ascending stairs. The average maximum plantar and dorsiflexion angles observed when descending were of 40° and 21° respectively. Accordingly, for the ascending motion, a plantarflexion angle of 31° and a dorsiflexion angle of 11° were observed.

Third, the STS ROM was obtained from the paper of M. K.Y. Mak et al. [24]. To measure this range they recorded the ankle angle of healthy patients and Parkinson patients. And since almost solely dorsiflexion occur in the STS motion only this value was reported. The maximum value was of 10.7° . From the first two studies, it can be seen that the angle in plantarflexion is always higher than in dorsiflexion. Based on this information a conservative plantar and dorsiflexion angle of 35° and 20° respectively were chosen.

A.2 Weight

R. L. Waters et al. found that an increase of O₂ consumption of 30% can be seen with an additional weight of 2 Kg to the ankle but if 20 Kg is added to the waist, little to no increase is perceived [25]. Additionally, since the Achilles exoskeleton weight 1.5 Kg and the lightest autonomous exoskeleton found in the literature review (PPAFO) weights 0.68 Kg the desired weight for the exoskeleton was set to lower than 1.5 Kg [15, 2].

A.3 Torques

Maximum walking plantarflexion torque was defined based on information found in the kinematic data gathered by Crowell H.P. et al. [26]. Furthermore, the maximum walking dorsiflexion torque was found on the paper of Brockett C.L. et al.[27]. As for the data of the maximum plantar and dorsiflexion torques for the stairs motion, the values were found in the paper of Vallabhajosula S. et al.[28]. Max Ankle torque for STS motion was found also in the paper of M. K.Y. Mak et al. [24]. One thing to note is that in walking, ascending and descending stairs the observed dorsiflexion torque is always significantly lower than the torque applied in plantarflexion.

A.4 Stair dimensions

One of the most significant limitations of the Achilles exoskeleton is the length and position of its lever arm because the lever arm is too long that it hits the stair step behind the leg when the user is descending. Hence, to define a maximum lever arm length, the stair dimensions in which the device should function need to be established. Thus the International standard for stairs was used for this purpose [29, 30].

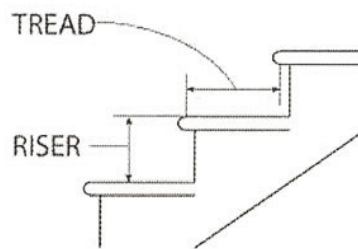


FIGURE A.1: Stair dimensions nomenclature.

A.5 Design dimensions

A requirement of this project is that the exoskeleton has to be able to climb and descend stairs and because of that the structure and parts of the device need to be maintained as close to the leg as possible so that collisions with the environment do not occur.

To assure that, it is necessary to analyze some possible problems that could arise depending on the device's dimensions. First, in the posterior lower limb space, it is already known from the Achilles design, that having a long lever arm in this place is a problem to descend stairs. Hence, this space will be limit to prevent that any possible design part hit the stair dimensions defined in A.4. Second, in the lower limb space, it is thought that adding an actuator in this place would help to expand the dorsiflexion ROM; however, there is also the possibility that the actuator hits a stair step. As a result, it is decided that any structure that could be located in the anterior lower limb space has to be kept just above the toe point.

Third, to determine an appropriate dimension for the internal lower limb space information found in the study from R.L. Kirby et al. was used [31]. In this paper they observed the effect of different stand positions on standing balance. For that, they recorded postural sway data of normal subject and patient with musculoskeletal problems. The data was then derived and expressed as the total travel of the center of pressure (CoP) in the Anterior-Posterior (AP) and Medio-Lateral (ML) directions and the mean AP and ML position of the CoP.

Their results showed that although separating the feet's in a stand-up position does reduce the mediolateral travel compared when they are together, increasing the separation distance above 15 cm would not further reduce the mediolateral travel nor will significantly affect the ML and AP mean position of the CoP (A.2). Since it seems body sway and the position of the CoP are not significantly affected by increasing the distance between the leg, it can also be assumed that balance will not be affected. Hence, an arbitrarily limit of maximum 20 cm of separation space between the legs was considered for the design limitations of the exoskeleton. However, ideally, this space should not be used for any component of the exoskeleton as to prevent any collision between them and the legs.

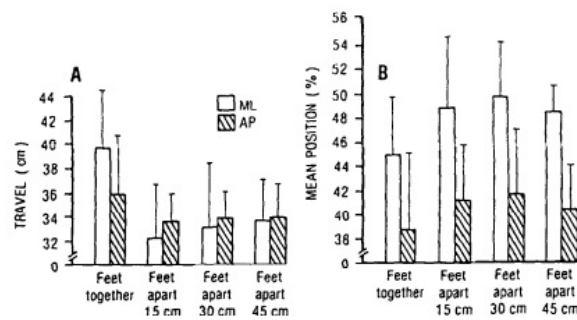


FIGURE A.2: Influence of medio-lateral variation of foot position (a) on travel expressed in cm and (b) on the mean position of the center of pressure expressed as a percentage of the distance from the midline (line connecting the mid heel to the second toe) of the right and left foot and from the heels to the toes [31].

Lastly, for the external space, no specific limitation was defined, since there is no problem that any possible parts get in the way with the stairs or the leg as they are not in line with the direction of motion.

Considering the previously mentioned information a delimitation area for the maximum dimensions of the exoskeleton was defined. This area not only is set to prevent motion collisions but also to create a final exoskeleton design as user-friendly as possible. A complete illustration of the limits is presented in Figure A.3.

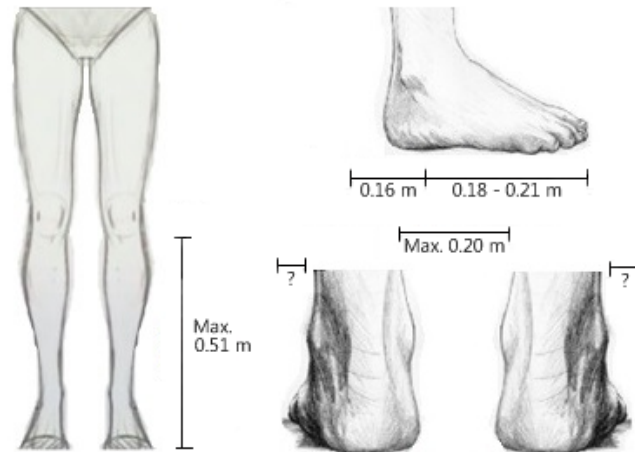


FIGURE A.3: Exoskeleton design area limitations

A.6 Pressure pain threshold

To prevent that the device produces discomfort or pain in the user a maximum limit of pressure is set for the possible fixing areas of the actuator. The anterior and posterior limits were obtained from the paper of J.C. Moreno et al. [32]. As for the pressure limits of the sole and dorsum, they were obtained from the paper of S. Xiong et al.[33].

The value chosen as the maximum PPT of the sole and dorsum were the values of the weakest points found in the same paper. These values were chosen as a measure to prevent any possible discomfort. The PPT value for the dorsum area in the paper of Moreno et al. lies between the ranges found in the paper of Xiong et al. Thus, it is assumed it is a reasonable estimation for this limitations.

A.7 Minimum angular velocity

To determine the minimum angular velocities in gait information from the book "Biomechanics and Motor Control of Human Movement 2nd edition" of D.A. Winter was used [18]. Furthermore, to collaborate with the results reported in the book, a manual estimation of the instantaneous angular velocity value was performed using the angular position dataset *theta_ankle_normal* from the same book. For the estimation, it was assumed that the time from a single step cycle was of 1.5 s. The obtained angular velocity values can be seen in the Figure A.4.

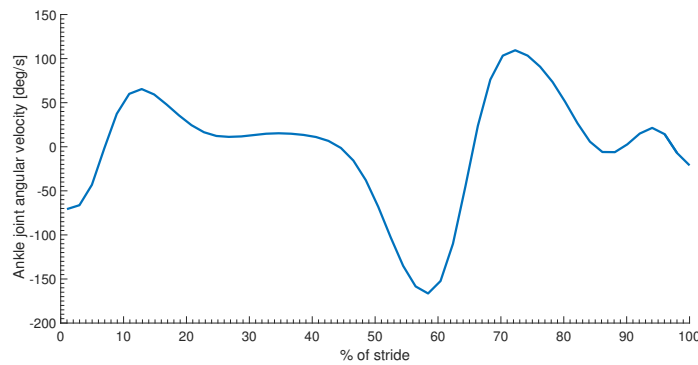


FIGURE A.4: Estimated angular velocity. The peak instantaneous angular velocity value is of 166.5 deg/s and correspond to the end of the stance phase.

From the obtained results an arbitrary value for the minimum plantar and dorsiflexion walking angular velocity was chosen. Minimum values for the angular velocities in stair climbing were obtained from [34]. Although the device is mainly focused on assisting walking and stair climbing, it is also essential to consider the angular velocities in the STS motion, as observed in [35] they tend to be considerably lower than in walking. Hence, precaution needs to be taken.

A.8 Degrees of freedom

Although allowing free movement on the frontal frame could increase the general performance of the design it was decided that the design would only have a single degree of freedom (plantar and dorsiflexion).

As a result, the design will be fixed so that there is no motion in the transversal plane (internal and external rotation) and the frontal plane (inversion and eversion). However, the consequences of fixing these two degrees of freedom will still be further investigated in the final phase of the project, as in can be seen in Figures A.5 and A.6, movement in the transversal and frontal plane contribute significantly to the natural motion of stair climbing [20].

It is expected that the perceived comfort of the user would be one of the parameters most affected by this decision. However, is still need to be investigated, if the motion of the sagittal plane would compensate for the absences of movement of the others planes in the motion performance.

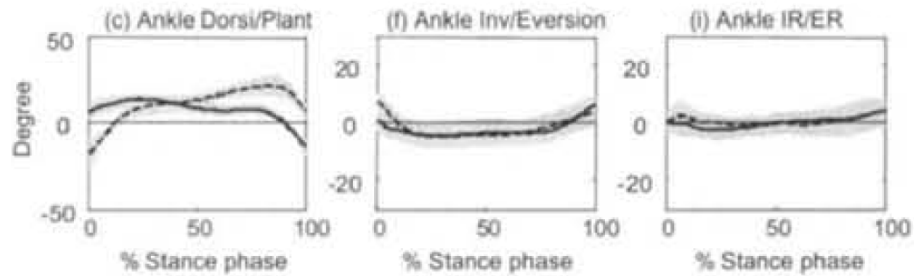


FIGURE A.5: Average joint angles in the sagittal, frontal and transversal planes during stance phase of stair ascent (solid lines) and descent (dashed lines) [20].

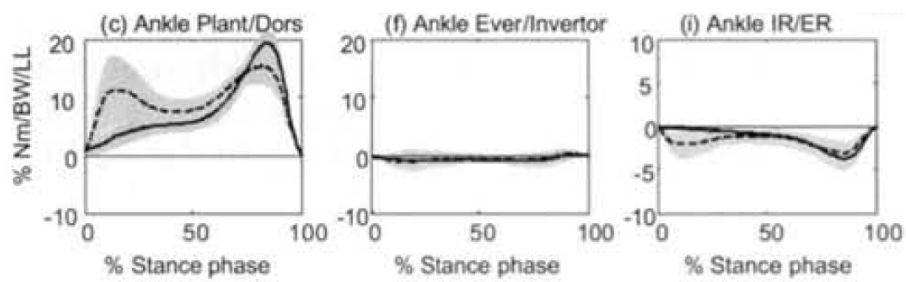


FIGURE A.6: Moments in the sagittal, frontal and transversal planes during stance phase of stair ascent (solid lines) and descent (dashed lines) [20].

B | Concept design analysis equations

Appendix B present the lists of the trigonometric equations of each individual concept in chapter 2 . The equation shown in the sections below are based on the free body diagrams seen in figure 2.1.

B.1 Concept 1 equations

$$\Theta_1 = \arcsin \frac{L_t}{L_2} \quad (\text{B.1})$$

$$\Theta_2 = \frac{\pi}{2} - \Theta_1 \quad (\text{B.2})$$

$$\beta_1 = \arcsin \frac{L_b}{L_1} \quad (\text{B.3})$$

$$\alpha_3 = \pi - \beta_1 - \Theta_2 \quad (\text{B.4})$$

$$\alpha_1 = \arcsin \frac{L_1 \sin(\alpha_3)}{L_a} \quad (\text{B.5})$$

$$L_1 = \sqrt{L_b^2 + L_s^2} \quad (\text{B.6})$$

$$L_2 = \sqrt{L_f^2 + L_t^2} \quad (\text{B.7})$$

$$L_a = \sqrt{L_1^2 + L_2^2 - 2L_1L_2 \cos(\alpha_3)} \quad (\text{B.8})$$

$$r = L_2 \sin(\alpha_1) \quad (\text{B.9})$$

$$F_a = \frac{T_o}{r} \quad (\text{B.10})$$

$$v_a = \dot{L}_a(t) \quad (\text{B.11})$$

$$P_a = F_a v_a \quad (\text{B.12})$$

B.2 Concept 2 equations

$$\Theta_2 = \arcsin \frac{L_b}{L_1} \quad (\text{B.13})$$

$$\alpha_2 = \frac{\pi}{2} - \theta_2 \quad (\text{B.14})$$

$$\alpha_1 = \pi - \alpha_2 - \alpha_3 \quad (\text{B.15})$$

$$\alpha_3 = \arcsin \frac{L_r \sin(\alpha_2)}{L_a} \quad (\text{B.16})$$

$$L_1 = \sqrt{L_b^2 + L_s^2} \quad (\text{B.17})$$

$$L_a = \sqrt{L_1^2 + L_r^2 - 2L_1L_r \cos(\alpha_2)} \quad (\text{B.18})$$

$$r = L_r \sin(\alpha_1) \quad (\text{B.19})$$

$$F_a = \frac{T_o}{r} \quad (\text{B.20})$$

B.3 Concept 3 equations

$$\Theta_2 = \arcsin \frac{L_f}{L_2} \quad (\text{B.21})$$

$$\phi_1 = \arctan \frac{L_b}{L_s} \quad (\text{B.22})$$

$$\phi_2 = \pi - \theta_2 \quad (\text{B.23})$$

$$\alpha_2 = \phi_2 - \phi_1 \quad (\text{B.24})$$

$$L_1 = \sqrt{L_b^2 + L_s^2} \quad (\text{B.25})$$

$$L_2 = \sqrt{L_f^2 + L_t^2} \quad (\text{B.26})$$

$$L_a = \sqrt{L_1^2 + L_2^2 - 2L_1L_2 \cos(\alpha_2)} \quad (\text{B.27})$$

$$r = L_2 \sin(\alpha_1) \quad (\text{B.28})$$

$$F_a = \frac{T_o}{r} \quad (\text{B.29})$$

C | Orthosis design process

Appendix C first present a description of the advantage and disadvantage of the individual components conforming the morphological chart in chapter 3. Second, the results of the FME analysis used to determine the resistance of the device hinges are shown. Lastly, the technical drawings used to fabricate the final prototype parts are provided.

C.1 Morphological chart-functions and solutions description

- Fastener method: the solution should firmly hold the parts of the orthosis body on the human limb as to keep them in place during movements of the leg.

S1. Velcro straps: these bands are a conventional material used in ankle and foot orthosis due to its relatively low cost and also because they are an excellent way to fasten fabric and other materials. However, they wear quickly, so periodic maintenance is required.

S2. Belts: these pieces of wear are a convenient way to fasten objects because they are found in many sizes and materials in the market. However, the belt's buckle creates a concentration pressure point that can generate discomfort.

S3. Boa laces: the boa lace system consist of a lightweight, super strong wire and a knob to adjust the tightness of the cable. Boa laces perform well to fasten footwear; however, they need periodic maintenance to keep the cable and the internal parts of the knob clean.

S4. Pressure buttons: these buttons are another common tool to fasten fabric. They hold objects well under most circumstances, and they use little to no space. However, they are not adequate to be used in projects were tightness needs to be variable.

S5. Compression sleeve: this solution is a fabric made of a robust and flexible material. Compression sleeves are quite comfortable to wear as they adapt to the form of the limb. Nevertheless, due to their flexibility, there is always a bit of movement between the held part and the sleeve. Hence, they are not a good choice for projects that require a stable structure.

- Upper force distribution:

S1. Part(s) on the side: semi-rigid or rigid plates typically collocated to patients with ankle instability. The plates allow a person to perform plantar and dorsiflexion but prevent it from performing high external and internal rotation. And they do not cover areas of the leg that can withstand high pressure.

S2. Part(s) on the back: shell plate(s) of semi-rigid or rigid material. These plates are the most common body structures found in ankle exoskeletons as typically the actuator and other components are fixed on the back of the shin. However, they tend to be uncomfortable when walking because the shells are located around the calf muscles.

S3. Part(s) on the front: shell plate(s) of semi-rigid or rigid material. These shells are typically used as shin protectors in sports. A frontal shell will need more padding or be made of a more resistant material than a posterior shell because the shin area has less muscle tissue covering the front of the lower leg. Hence, making it more sensitive. Furthermore, because the actuator force is directly applied to the shell, it is possible that discomfort is perceived due to a pressure focus point.

- Lower force distribution:

S1. Foot top: plate(s) used to support the foot of patients suffering from foot drop. The plates cover a sensitive area of the foot, so applying a force here will inevitably produce some discomfort.

S2. Foot sole: these plates are widely used in foot orthosis and exoskeletons because the force applied in the sole can be dissipated to the ground. However, they can also limit the natural bending movement of the foot.

- Shank/foot hinge:

S1. One-sided hinge: single hinge structures are frequently used in passive exoskeletons. A single hinge work great to provide support to the leg without sacrificing much comfort. However, these structures are prone to structural instabilities because most of the leg weight and the forces acting on it are focused only on one side of the leg.

S2. Double-sided hinge: This structure provides excellent support for ankle orthosis. However, they are uncomfortable to wear, because they limit the natural motion of the foot.

C.2 Hinges FME Analysis

Figures C.1 and C.2 show the results for a single and dual actuator arrangement using an equal pin diameter of 10 mm for the exoskeleton's shin and footplate hinges respectively. In both static analysis the lateral plates are defined as fixed and a Total force of 1300 N is applied to the actuator connector part. In the dual actuator arrangement each actuator deliver half of the total actuator force.

In both Figures C.1 and C.2 it can be clearly seen that in the single actuator case not only the maximum stress occurs in the area the force is being applied, but also that its magnitude is significantly greater than the material maximum yield stress, meaning that the pin will be deformed. In contrast, by using two actuators all structure stresses are maintained significantly below the yield strength value. Hence, the decision of distributing the force into two actuators.

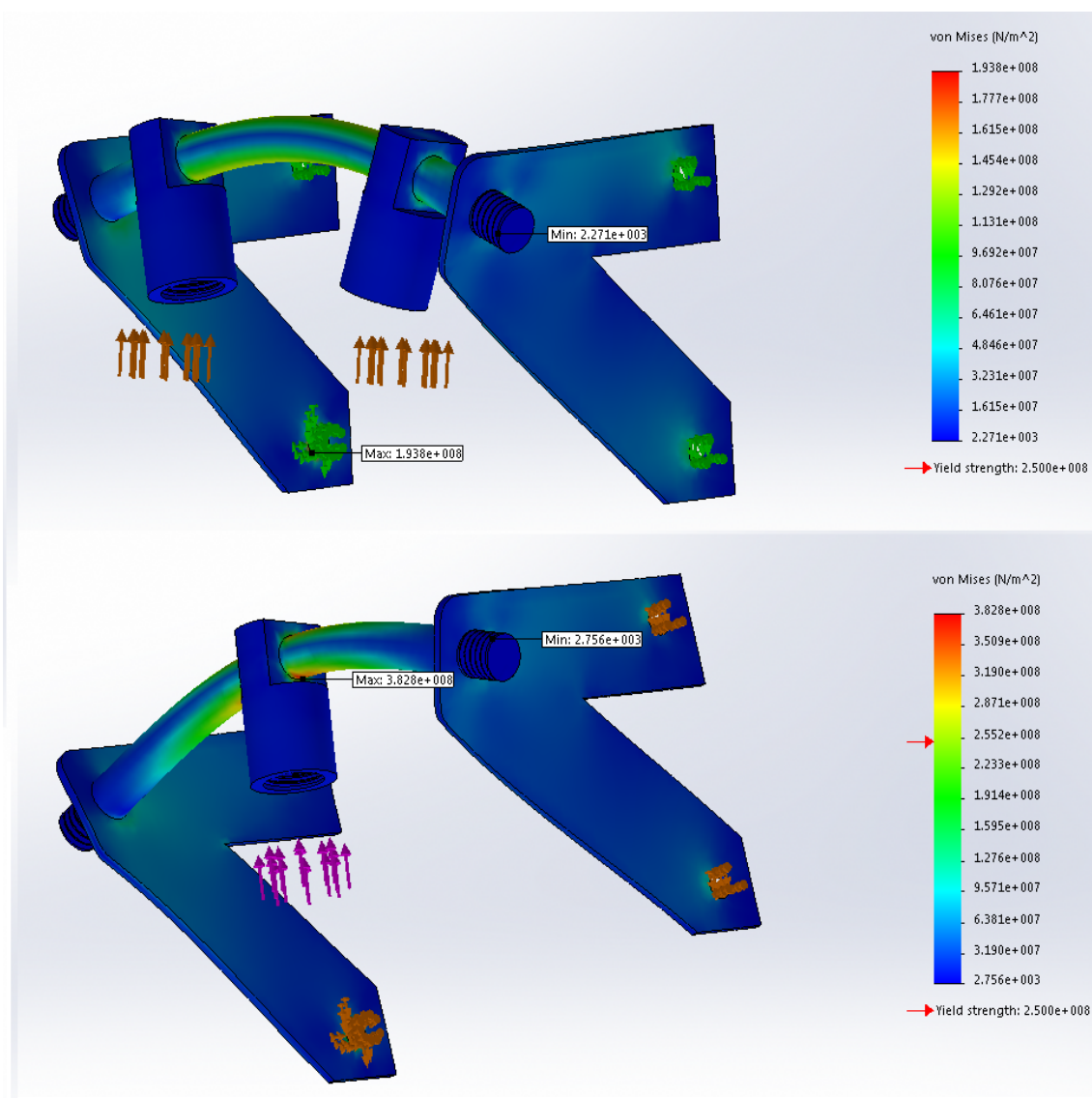


FIGURE C.1: Shin-hinge von Mises Stress results for single actuator (bottom) and dual actuator (Top) arrangement.

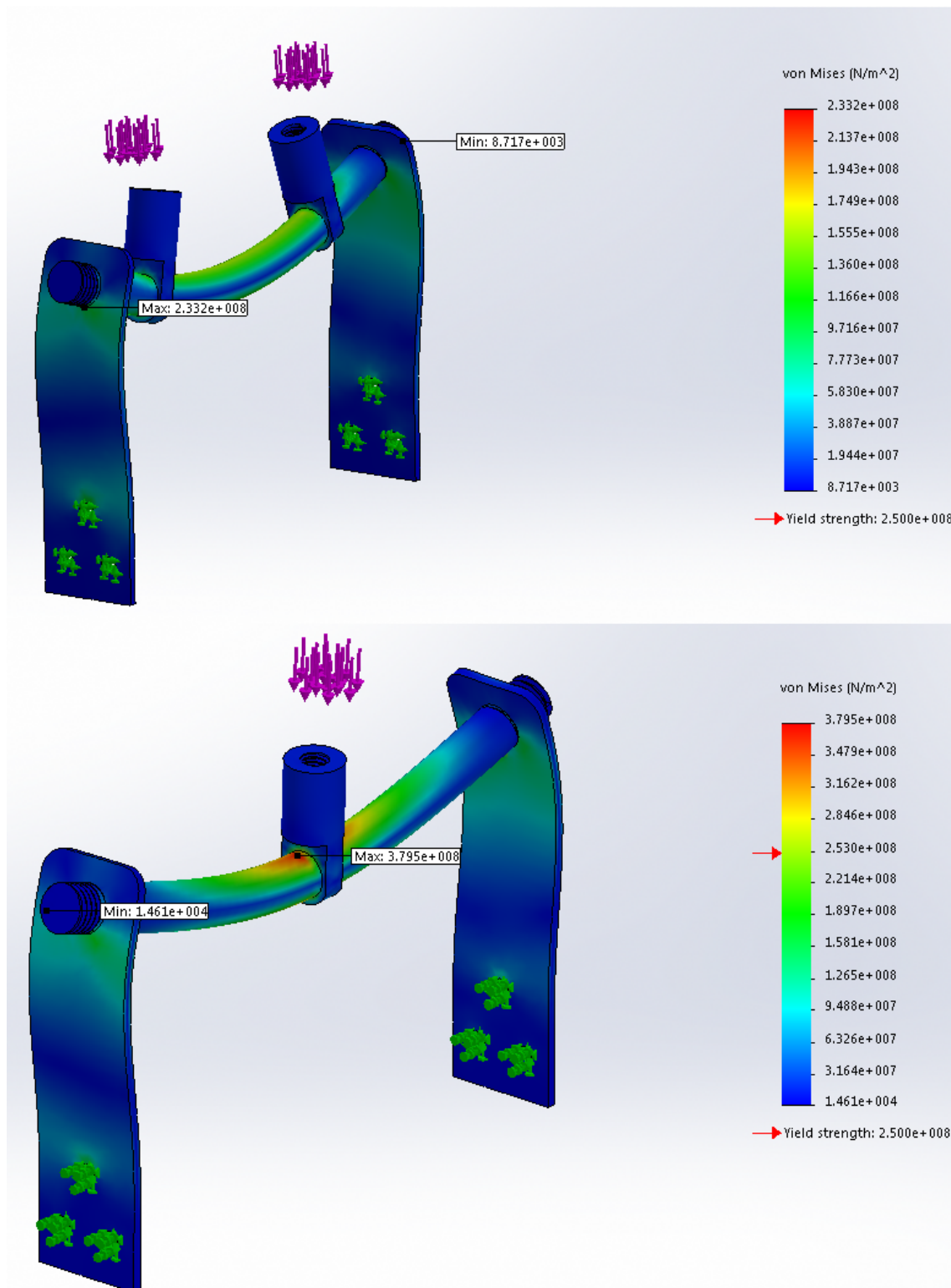


FIGURE C.2: Footplate-hinge von Mises Stress results for single actuator (bottom) and dual actuator (Top) arrangement.

C.3 Prototype's technical drawings

In the following pages, the detailed technical drawings of the parts that conform the ankle exoskeleton prototype are presented. The dimensions shown in the laser cut parts are meant for the metallic sheet plates necessary for its fabrication. Other dimensions are by default specified in their respective DXF files included in the CD provided with this report.

6 5 4 3 2 1

D

D

C

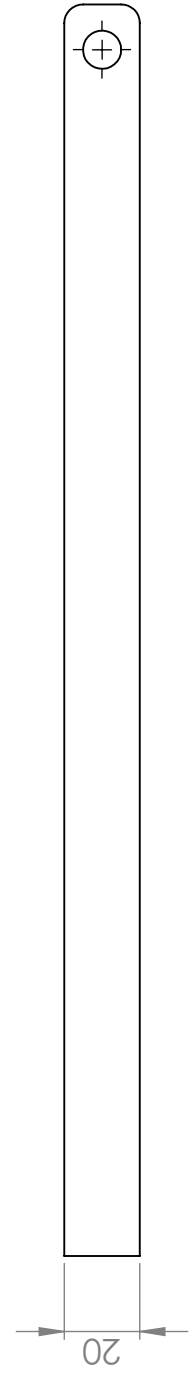
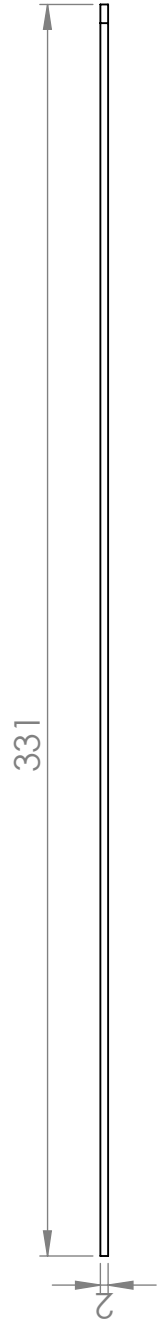
C

B

B

A

A



UNLESS OTHERWISE SPECIFIED: DIMENSIONS ARE IN MILLIMETERS SURFACE FINISH: TOLERANCES: +0.1 LINEAR: ANGULAR:		FINISH:	DEBURE AND BREAK SHARP EDGES		DO NOT SCALE DRAWING	REVISION
						1
NAME	SIGNATURE	DATE	TITLE:			
DRAWN	Jesus	13-9-2018	bars on the side of the shell			
CHK'D			DWG NO.			
APP'VD			side-bar-final			
MFG			A4			
Q-A			MATERIAL: STEEL ST37			
			SCALE: 1:5			
			WEIGHT:			

This part is meant to be laser cut.
Please see the DXF file for the full dimensions.

6 5 4 3 2 1

SHEET 1 OF 1

D

C

B

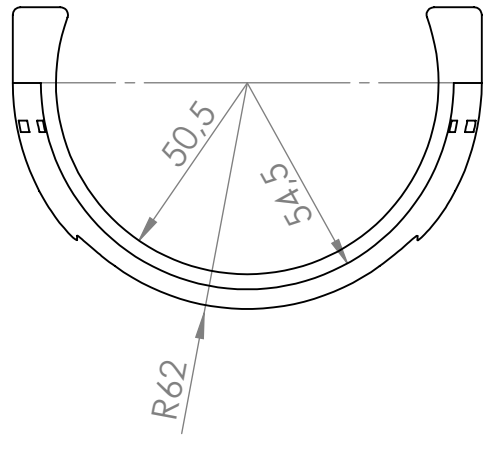
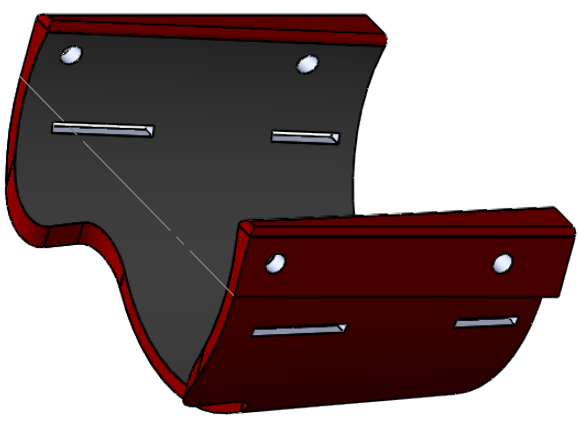
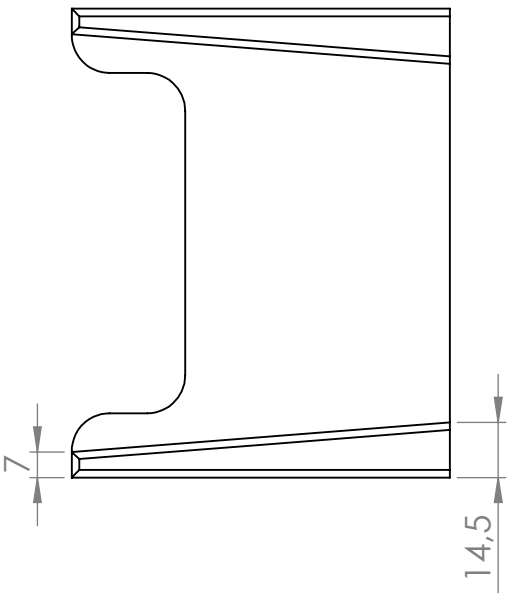
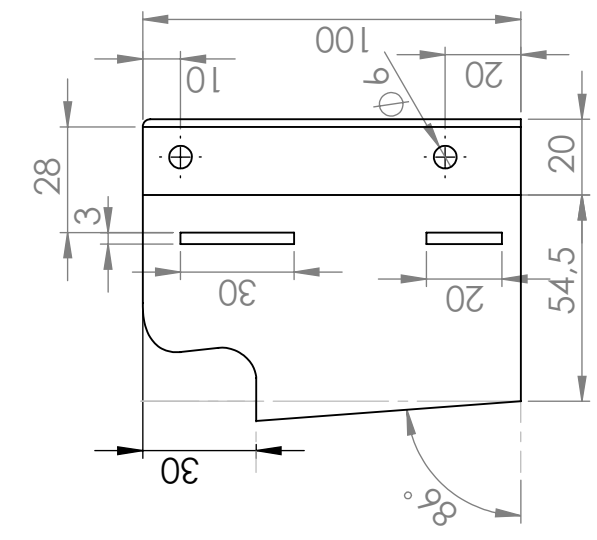
A

D

C

B

A



UNLESS OTHERWISE SPECIFIED: DIMENSIONS ARE IN MILLIMETERS		FINISH:		DEBURR AND BREAK SHARP EDGES		DO NOT SCALE DRAWING		REVISION	
SURFACE FINISH:		/						2	
TOLERANCES: +5									
LINEAR:									
ANGULAR:									
NAME	SIGNATURE	DATE	TITLE:						
DRAWN	Jesus	13-9-2018	Calve support						
CHK'D			DWG NO. A4						
APP'VD			MATERIAL: Fiberglass						
MFG			SCALE: 1:2						
Q.A			SHEET 1 OF 1						

6

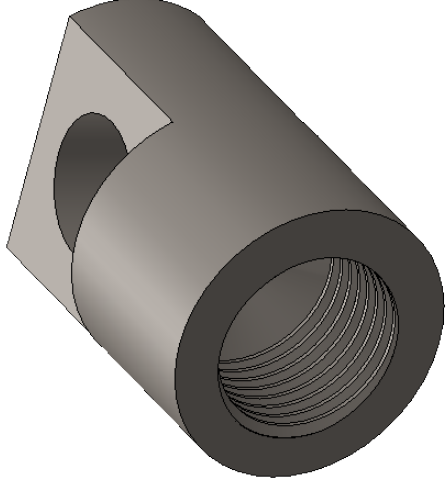
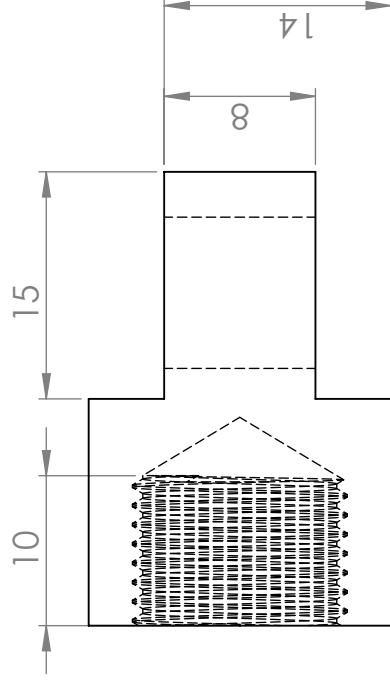
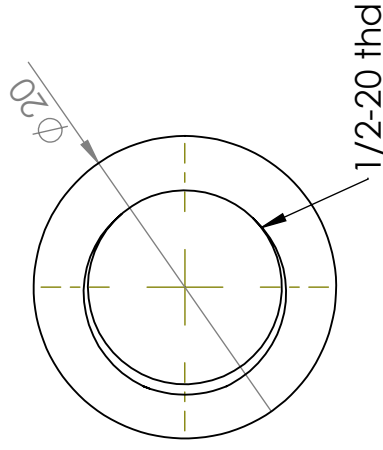
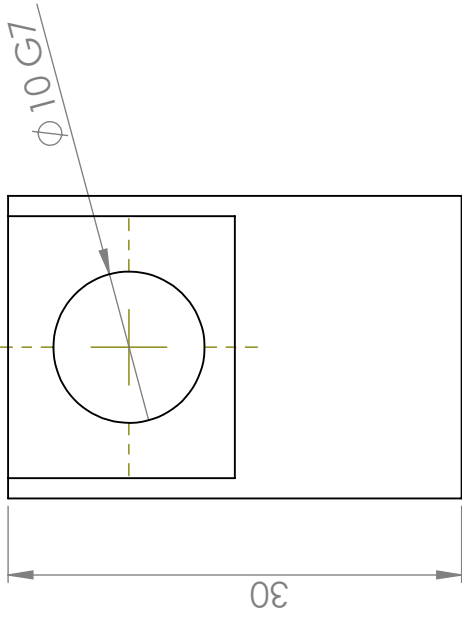
5

4

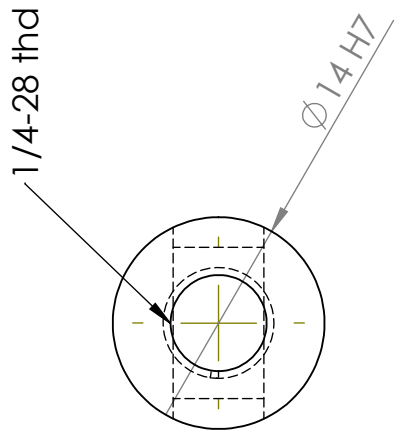
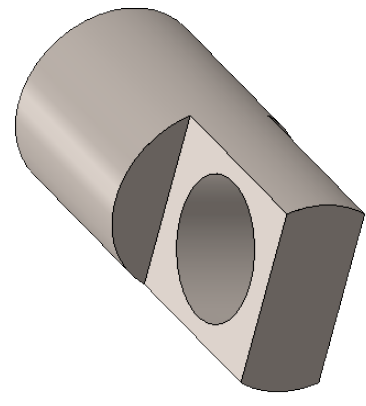
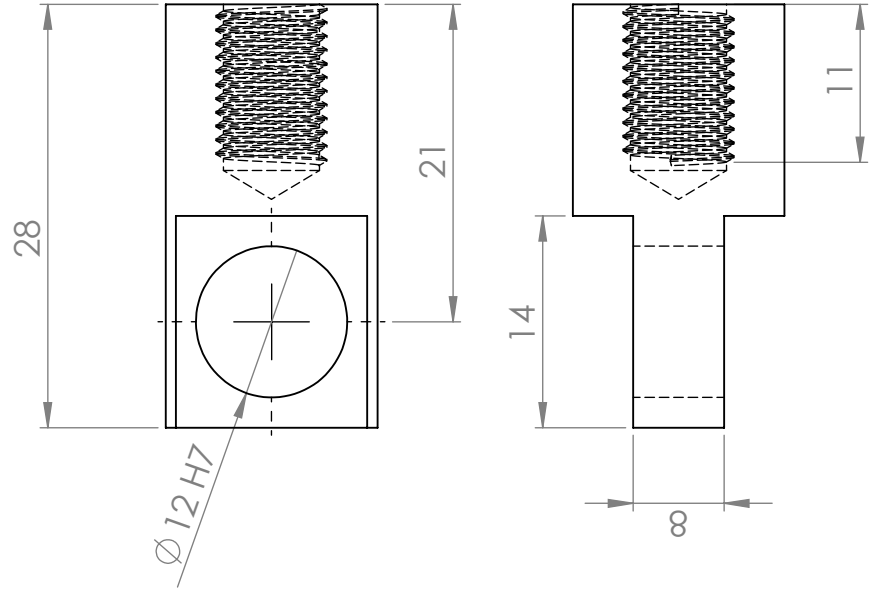
3

2

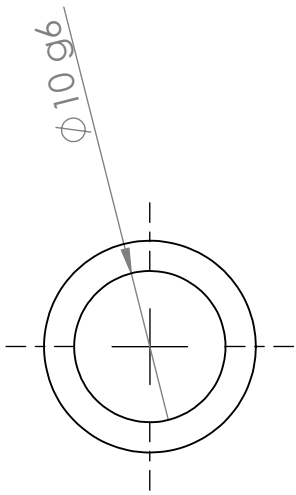
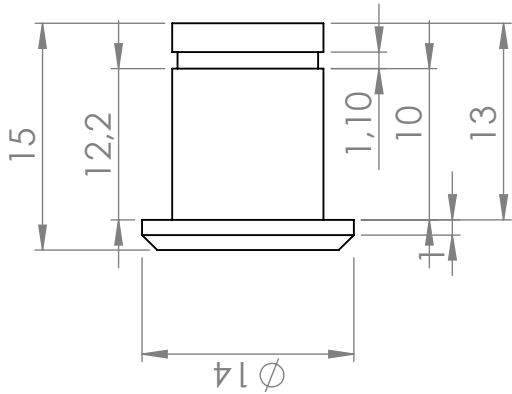
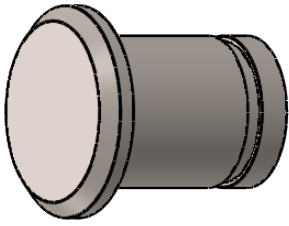
1



UNLESS OTHERWISE SPECIFIED: DIMENSIONS ARE IN MILLIMETERS		FINISH:		DEBURE AND BREAK SHARP EDGES		DO NOT SCALE DRAWING		REVISION	
SURFACE FINISH:		/						1	
TOLERANCES:									
LINEAR:									
ANGULAR:									
DRAWN	NAME	SIGNATURE	DATE						
CHK'D	Jesus		13-09-2018						
APP'VD									
MFG									
Q.A				MATERIAL:		Steel ST37		DWG NO. A4	
				TITLE:				cap to increase the top radius of the actuator	
				SCALE:2:1				SHEET 1 OF 1	



UNLESS OTHERWISE SPECIFIED: DIMENSIONS ARE IN MILLIMETERS		FINISH:		DEBURE AND BREAK SHARP EDGES		DO NOT SCALE DRAWING		REVISION	
SURFACE FINISH:		/						1	
TOLERANCES: ±0.1									
LINEAR:									
ANGULAR:									
DRAWN	NAME	SIGNATURE	DATE						
CHK'D	Jesus		13-09-2018						
APP'VD									
MFG									
Q.A									
				MATERIAL:		Aluminium		DWG NO. A4	
				WEIGHT:		SCALE: 2:1		SHEET 1 OF 1	
				TITLE:		flat eye to fix the actuator to the foot hinge			



UNLESS OTHERWISE SPECIFIED: DIMENSIONS ARE IN MILLIMETERS SURFACE FINISH: TOLERANCES:+0,1 LINEAR: ANGULAR:		FINISH:		DEBURE AND BREAK SHARP EDGES		DO NOT SCALE DRAWING		REVISION		1	
DRAWN Jesus		SIGNATURE		DATE 19-09-2018		TITLE: Pin going through the foot hinge		DWG NO. A4		SCALE:2:1	
CHK'D		MATERIAL:		WEIGHT:		SHEET 1 OF 1					
APP'VD											
MFG											
Q.A											

D

C

B

A

D

C

B

A

6

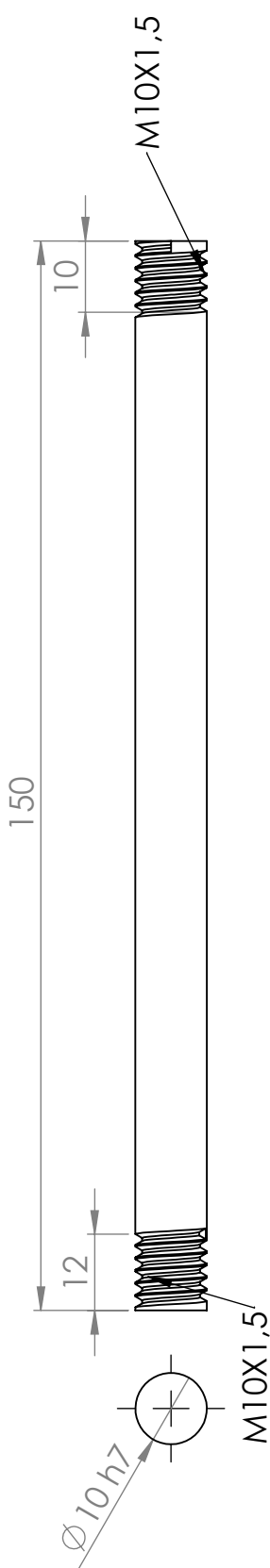
5

4

3

2

1



UNLESS OTHERWISE SPECIFIED: DIMENSIONS ARE IN MILLIMETERS SURFACE FINISH: TOLERANCES:-0,1 LINEAR: ANGULAR:		FINISH:		/		DEBURE AND BREAK SHARP EDGES		DO NOT SCALE DRAWING		REVISION		1	
DRAWN	NAME	SIGNATURE	DATE	MATERIAL: Steel ST37				TITLE: shin bracelet pin				DWG NO. A4	
CHK'D	Jesus		13-09-2018										
APP'VD													
MFG													
Q.A													
WEIGHT:				SCALE:1:2				SHEET 1 OF 1					

6

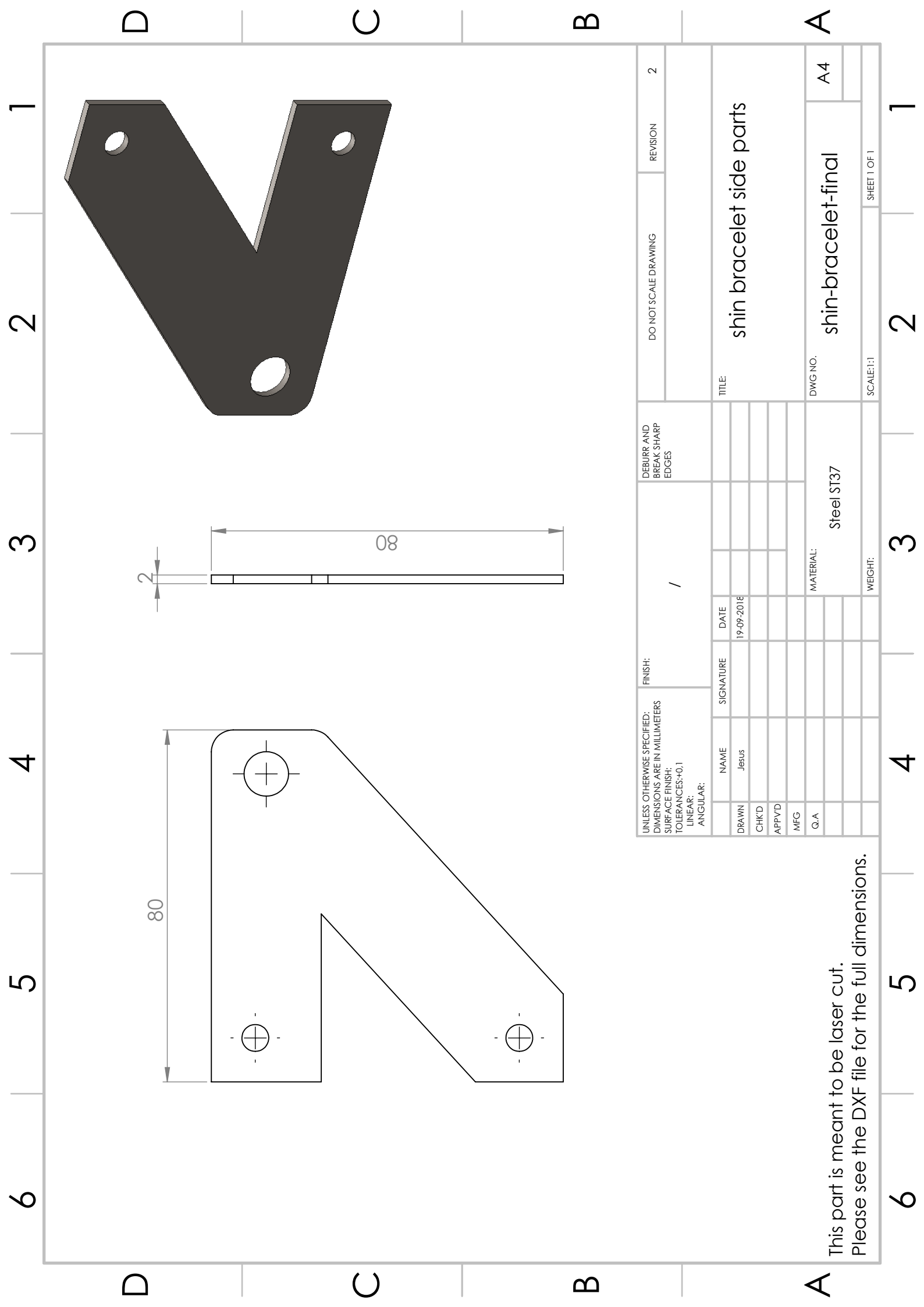
5

4

3

2

1



UNLESS OTHERWISE SPECIFIED: DIMENSIONS ARE IN MILLIMETERS SURFACE FINISH: TOLERANCES:+0.1 LINEAR: ANGULAR:		FINISH:		DEBURE AND BREAK SHARP EDGES		DO NOT SCALE DRAWING		REVISION		2	
DRAWN Jesus		SIGNATURE		DATE 19-09-2018		TITLE: shin bracelet side parts		DWG NO. shin-bracelet-final		A4	
CHK'D						MATERIAL: Steel ST37		SCALE:1:1		SHEET 1 OF 1	
APP'VD						WEIGHT:					
MFG											
Q.A											

This part is meant to be laser cut.
Please see the DXF file for the full dimensions.

6 5 4 3 2 1

D

D

C

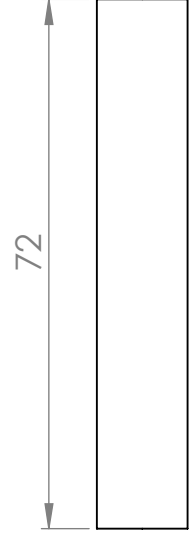
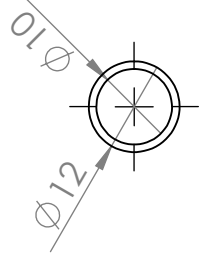
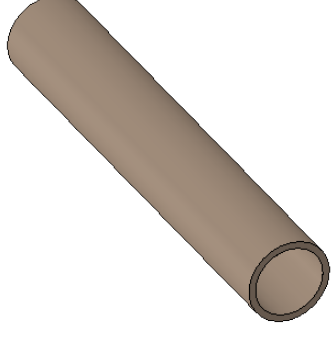
C

B

B

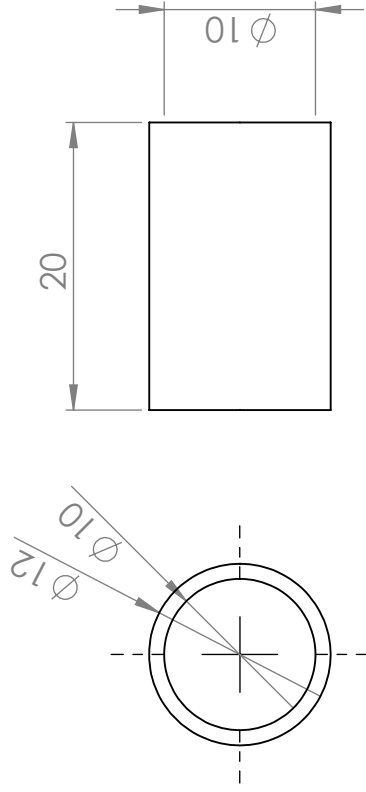
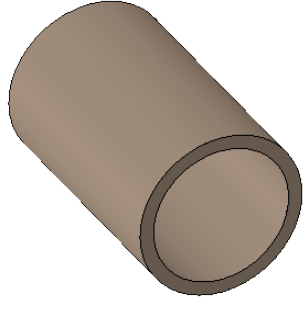
A

A

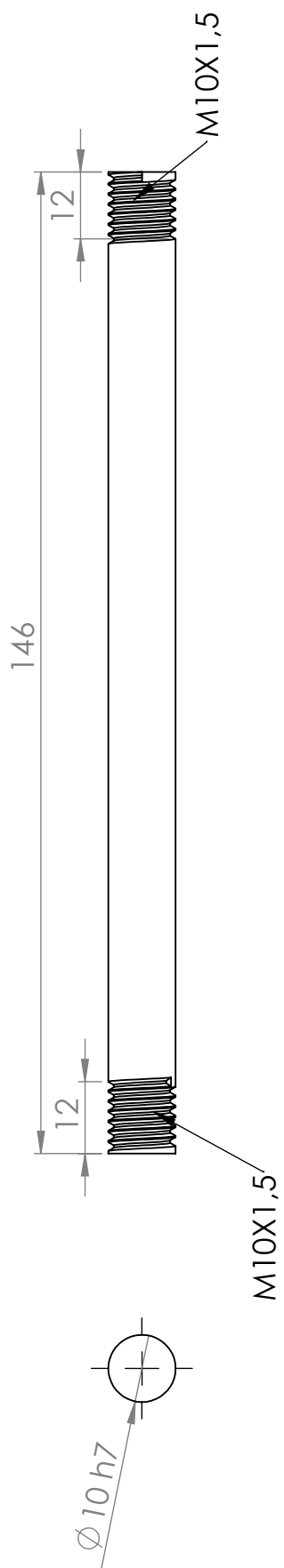


UNLESS OTHERWISE SPECIFIED: DIMENSIONS ARE IN MILLIMETERS		FINISH:		DEBURR AND BREAK SHARP EDGES		DO NOT SCALE DRAWING		REVISION	
SURFACE FINISH:		/						1	
TOLERANCES:-0.1									
LINEAR:									
ANGULAR:									
DRAWN	NAME	SIGNATURE	DATE						
CHK'D	Jesus		13-09-2018						
APP'VD									
MFG									
Q.A									
				MATERIAL:		DWG NO.		A4	
						shin-bracelet-middle-spacer			
						spacer to position the actuator in place			
				WEIGHT:		SCALE:1:1		SHEET 1 OF 1	

6 5 4 3 2 1



UNLESS OTHERWISE SPECIFIED: DIMENSIONS ARE IN MILLIMETERS SURFACE FINISH: TOLERANCES:-0.1 LINEAR: ANGULAR:		FINISH:	/		DEBURR AND BREAK SHARP EDGES	DO NOT SCALE DRAWING	REVISION	1
DRAWN	NAME	SIGNATURE	DATE	TITLE: spacer to position the actuator in place				
CHK'D	Jesus		13-09-2018	DWG NO. shin-bracelet-lateral-spacer				
APP'VD				SCALE:2:1				
MFG				SHEET 1 OF 1				
Q.A				MATERIAL:				
				WEIGHT:				



UNLESS OTHERWISE SPECIFIED: DIMENSIONS ARE IN MILLIMETERS		FINISH:		DEBURE AND BREAK SHARP EDGES		DO NOT SCALE DRAWING		REVISION	
SURFACE FINISH:		/						1	
TOLERANCES:-0,1									
LINEAR:									
ANGULAR:									
DRAWN	NAME	SIGNATURE	DATE						
CHK'D	Jesus		13-09-2018						
APP'VD									
MFG									
Q.A									
				MATERIAL:		TITLE:			
				Steel ST37		foot bracelet pin			
						DWG NO.		A4	
						SCALE:1:2			
				WEIGHT:		SHEET 1 OF 1			

1 2 3 4 5 6

D C B A

D C B A

1 2 3 4 5 6

6 5 4 3 2 1

D

D

C

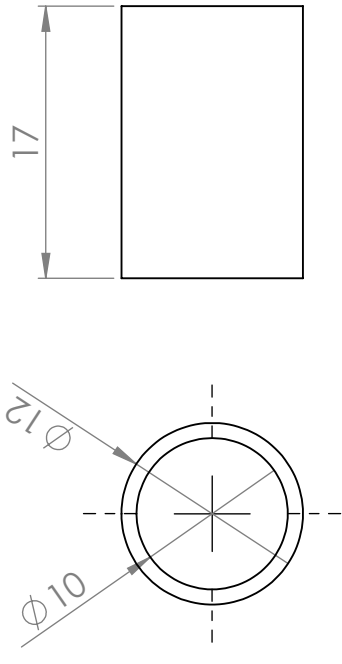
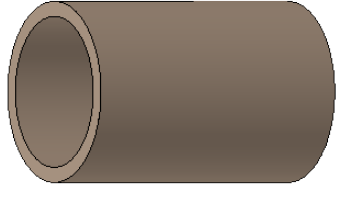
C

B

B

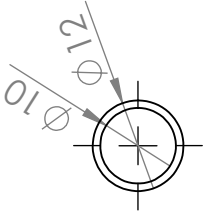
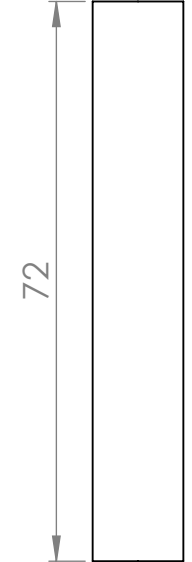
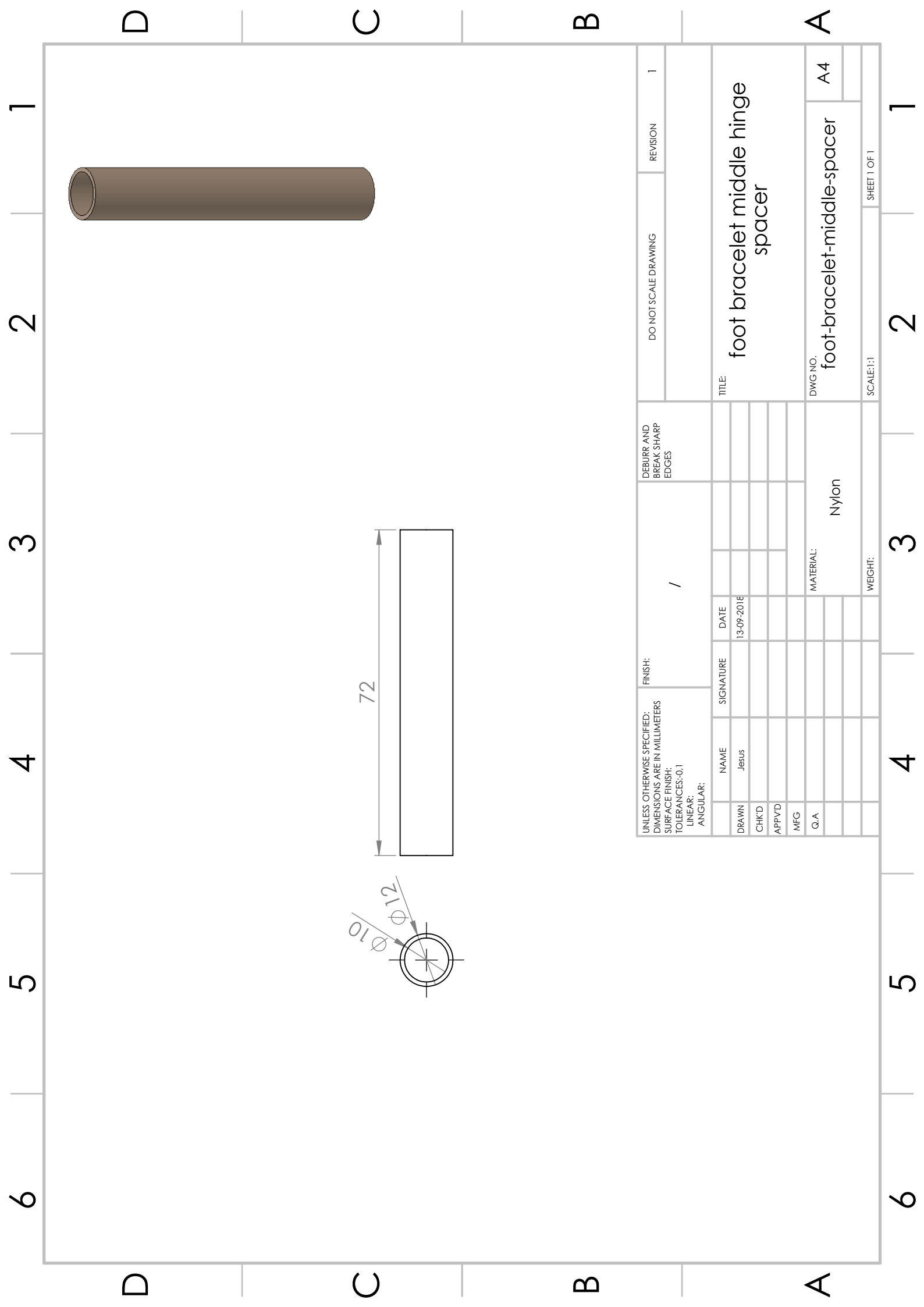
A

A

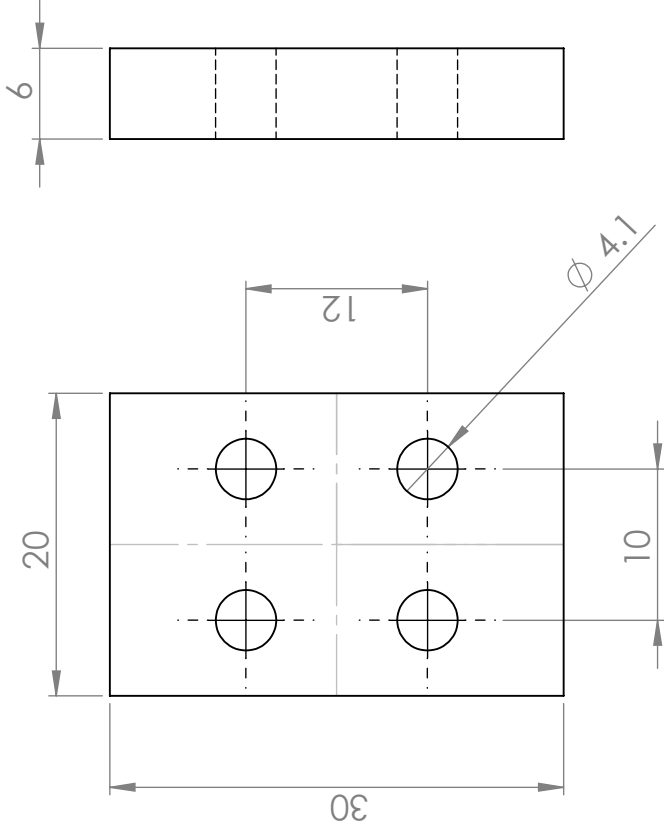
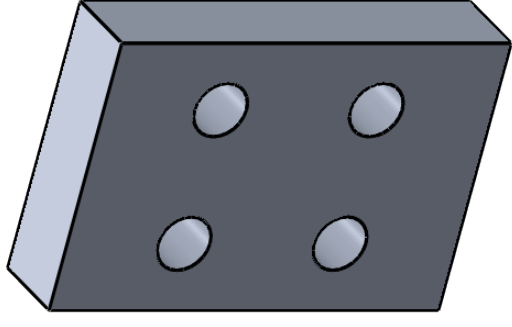


UNLESS OTHERWISE SPECIFIED: DIMENSIONS ARE IN MILLIMETERS		FINISH:		DEBURE AND BREAK SHARP EDGES		DO NOT SCALE DRAWING		REVISION		1	
SURFACE FINISH:		/									
TOLERANCES:											
LINEAR:											
ANGULAR:											
DRAWN	NAME	SIGNATURE	DATE								
CHK'D	Jesus		13-09-2018								
APP'VD											
MFG											
Q.A											
				MATERIAL:		Nylon		DWG NO.		A4	
								TITLE:		spacer to position actuator in the foot bracelet	
								SCALE:2:1		SHEET 1 OF 1	

6 5 4 3 2 1



UNLESS OTHERWISE SPECIFIED: DIMENSIONS ARE IN MILLIMETERS SURFACE FINISH: TOLERANCES:-0.1 LINEAR: ANGULAR:		FINISH:	/		DEBURE AND BREAK SHARP EDGES	DO NOT SCALE DRAWING	REVISION	1
NAME	SIGNATURE	DATE				TITLE: foot bracelet middle hinge spacer		
DRAWN	Jesus	13-09-2018				DWG NO. foot-bracelet-middle-spacer		
CHK'D						A4		
APP'VD								
MFG								
Q.A			MATERIAL: Nylon					
			WEIGHT:			SCALE:1:1		
			SHEET 1 OF 1					



UNLESS OTHERWISE SPECIFIED: DIMENSIONS ARE IN MILLIMETERS SURFACE FINISH: TOLERANCES:±0.1 LINEAR: ANGULAR:		FINISH:	/		DEBURR AND BREAK SHARP EDGES	DO NOT SCALE DRAWING	REVISION	1
DRAWN	NAME	SIGNATURE	DATE	TITLE: part to joint the metallic plates on the foot hinge				
CHK'D	Jesus		13-09-2018	DWG NO. A4				
APP'VD				MATERIAL: Aluminium				
MFG				SCALE:2:1				
Q.A				WEIGHT: SHEET 1 OF 1				

6 5 4 3 2 1

D

D

C

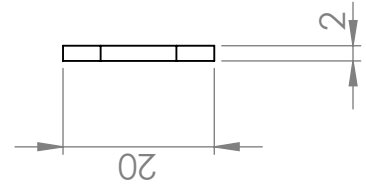
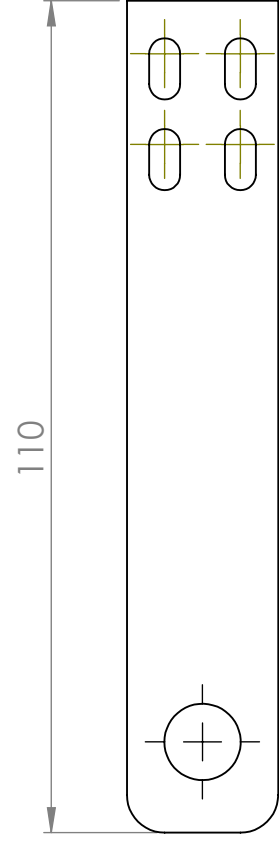
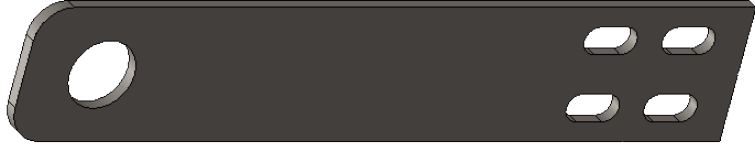
C

B

B

A

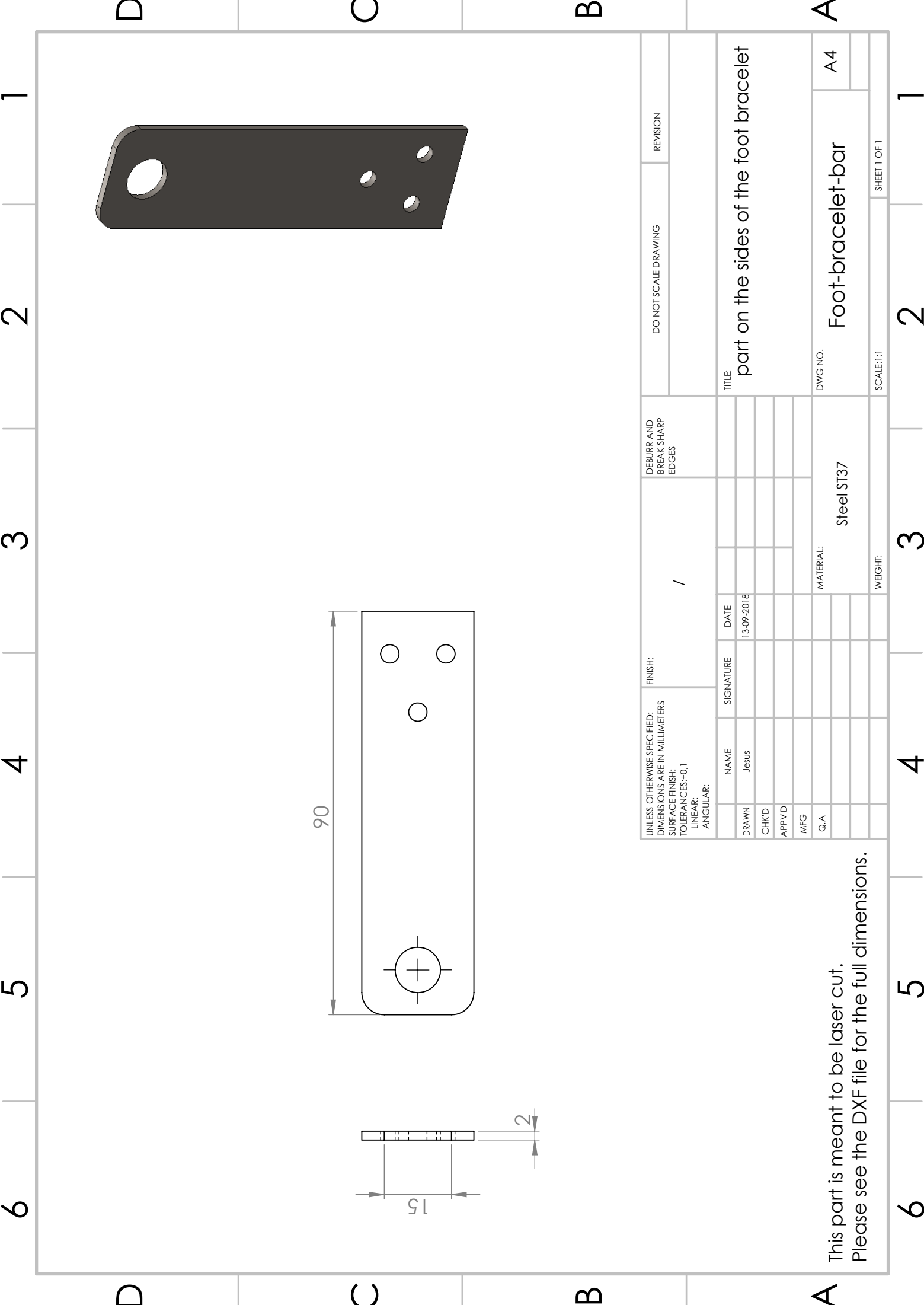
A



UNLESS OTHERWISE SPECIFIED: DIMENSIONS ARE IN MILLIMETERS SURFACE FINISH: TOLERANCES: +0.1 LINEAR: ANGULAR:		FINISH:	/		DEBURR AND BREAK SHARP EDGES	DO NOT SCALE DRAWING	REVISION	1
DRAWN	NAME	SIGNATURE	DATE	TITLE:		part conforming the foot hinge		
CHK'D	Jesus		13-09-2018	DWG NO.		A4		
APP'VD				MATERIAL:		Lower-body-internal-part-final		
MFG				Steel ST37		SCALE:1:1		
Q-A				WEIGHT:		SHEET 1 OF 1		

This part is meant to be laser cut.
Please see the DXF file for the full dimensions.

6 5 4 3 2 1



6 5 4 3 2 1

D C B A

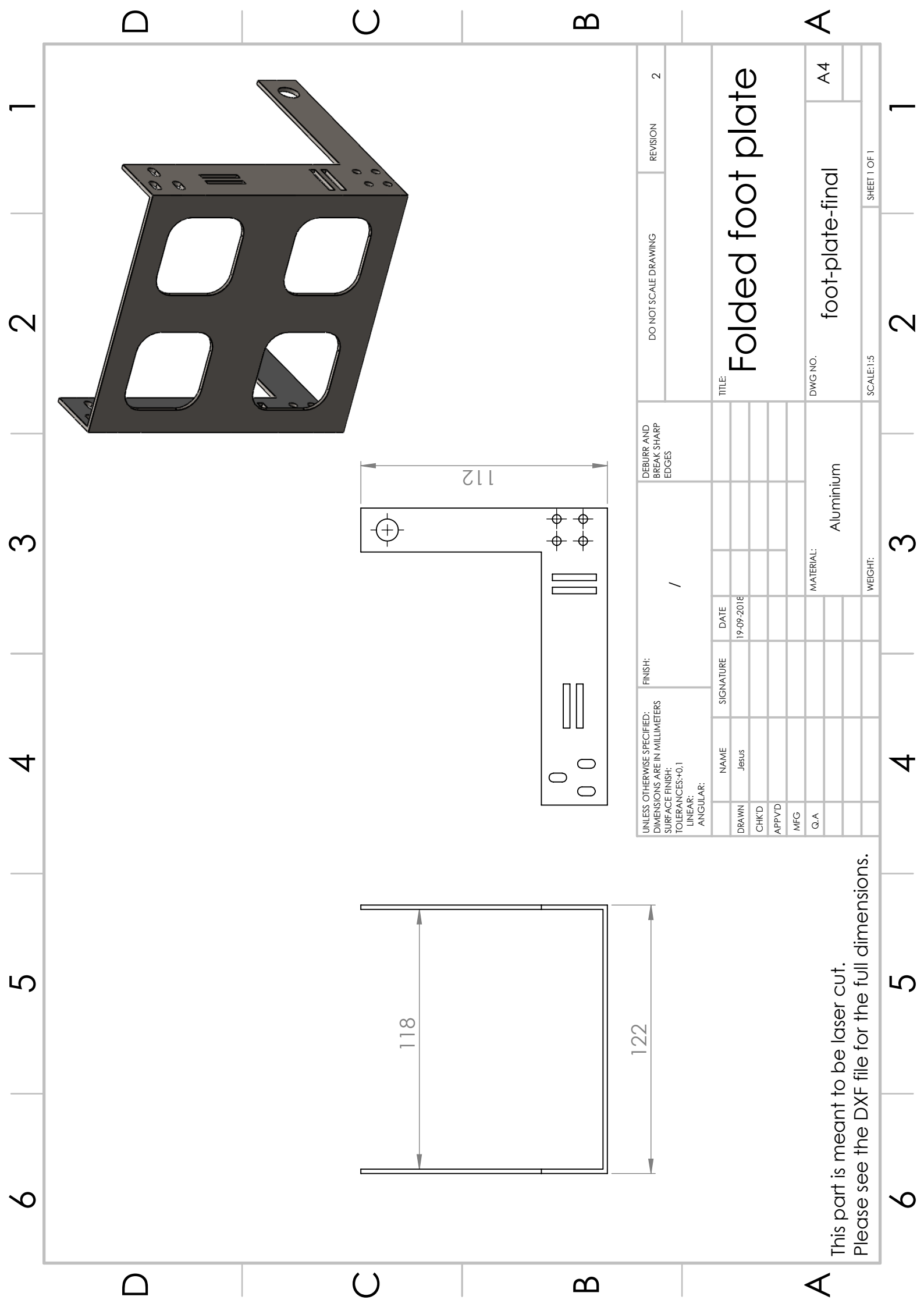
UNLESS OTHERWISE SPECIFIED: DIMENSIONS ARE IN MILLIMETERS		FINISH:		DEBURE AND BREAK SHARP EDGES		DO NOT SCALE DRAWING		REVISION	
SURFACE FINISH:		/							
TOLERANCES:+0,1									
LINEAR:									
ANGULAR:									
DRAWN	NAME	SIGNATURE	DATE						
CHK'D	Jesus		13-09-2018						
APP'VD									
MFG									
Q-A				MATERIAL:		Steel ST37		DWG NO. A4	
				WEIGHT:		SCALE:1:1		SHEET 1 OF 1	

TITLE: part on the sides of the foot bracelet

This part is meant to be laser cut.
Please see the DXF file for the full dimensions.

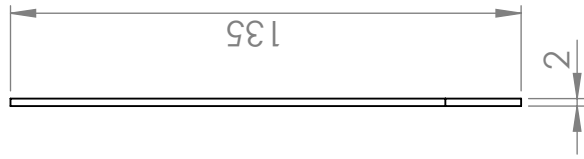
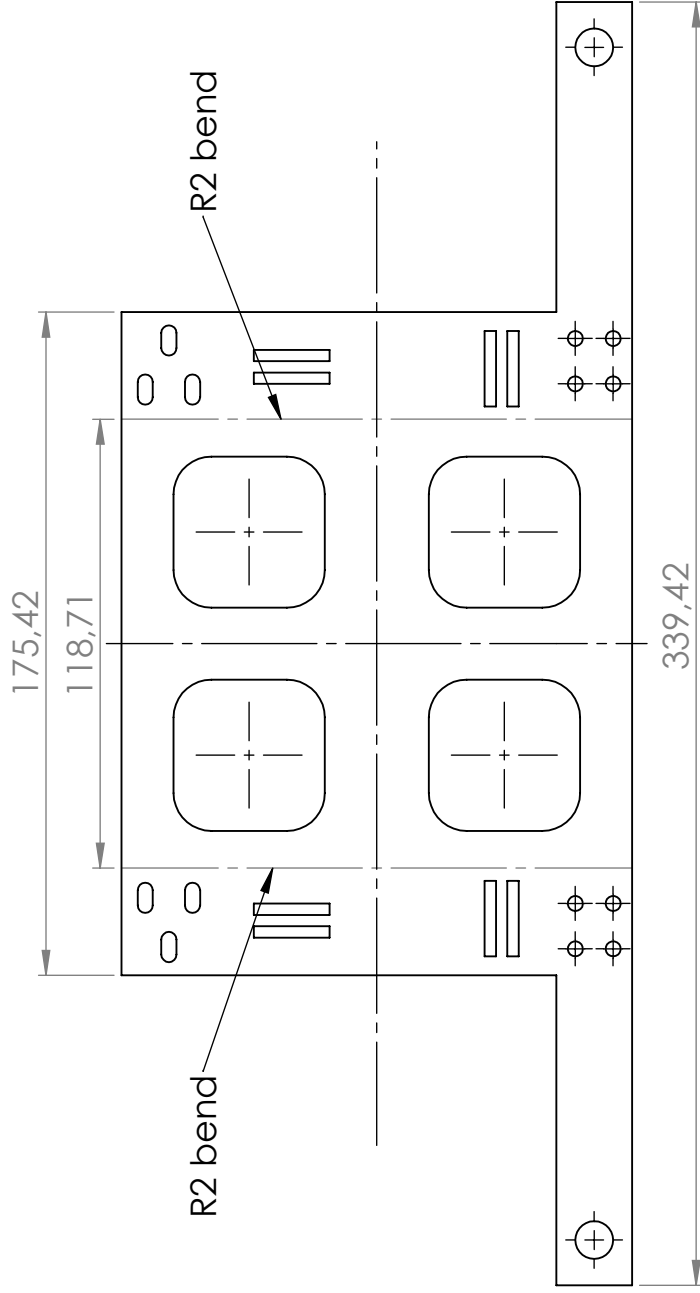
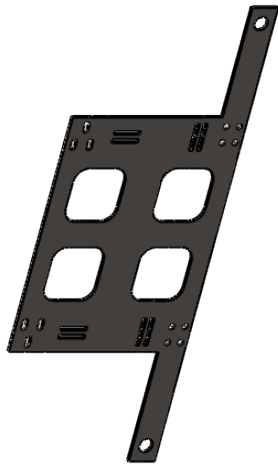
6 5 4 3 2 1

D C B A



UNLESS OTHERWISE SPECIFIED: DIMENSIONS ARE IN MILLIMETERS		FINISH:		DEBURE AND BREAK SHARP EDGES		DO NOT SCALE DRAWING		REVISION	
SURFACE FINISH:		/						2	
TOLERANCES:±0.1									
LINEAR:									
ANGULAR:									
DRAWN	NAME	SIGNATURE	DATE						
CHK'D	Jesus		19-09-2018						
APP'VD									
MFG									
Q.A									
				MATERIAL:		Aluminium		A4	
				DWC NO.		foot-plate-final			
				WEIGHT:		SCALE:1:5		SHEET 1 OF 1	
				TITLE:		Folded foot plate			

This part is meant to be laser cut.
Please see the DXF file for the full dimensions.



UNLESS OTHERWISE SPECIFIED: DIMENSIONS ARE IN MILLIMETERS		FINISH:		DEBURE AND BREAK SHARP EDGES		DO NOT SCALE DRAWING		REVISION	
SURFACE FINISH:		/						2	
TOLERANCES:±0,1									
LINEAR:									
ANGULAR:									
DRAWN	NAME	SIGNATURE	DATE						
CHK'D	Jesus		19-09-2018						
APP'VD									
MFG									
Q.A									
				MATERIAL:		Aluminium		A4	
				DWC NO.		foot-plate-final			
				WEIGHT:		SCALE:1:5		SHEET 1 OF 1	

Unfolded foot plate

This part is meant to be laser cut.
Please see the DXF file for the full dimensions.

D | Experiments illustrations and data

Appendix D present First, a Table D.1 containing the data that was recorded during the manual pump experiments. The stroke values in this table were used to estimate the ankle angle and moment arm at which each measurement was taken. In turn, the moment arm and force values were used to obtain the individual ankle torques. Second, a set of figures demonstrating the different ROM obtained in the experiments.

D.1 Manual pump test data

TABLE D.1: Ankle torque and measurements from the manual pump experiments

<i>Direction</i>	<i>Pressure [bar]</i>	<i>force [Kgf]</i>	<i>force [N]</i>	<i>Stroke [m]</i>	<i>Moment arm [m]</i>	<i>Ankle angle [°]</i>	<i>Torque [Nm]</i>
Dorsiflexion							
	2	0.8	7.84	0.008	0.2752	20.96	0.837
	5	2.2	21.56	0.0245	0.2869	12.626	2.439
	7	3.6	35.28	0.032	0.29	8.835	4.0539
	12	4.4	43.12	0.067	0.3088	-8.858	4.987
Plantarflexion							
	10	7.2	70.56	0.0125	0.2202	18.693	15.537
	20	14	137.2	0.015	0.2360	17.43	32.38
	30	20.6	201.88	0.0165	0.2442	16.67	49.292
	40	28	274.4	0.019	0.2569	15.406	70.50
	50	29.8	292.04	0.021	0.2659	14.395	77.66
	80	38.2	374.36	0.045	0.3096	2.263	115.904

Note: A negative ankle angle represent an angle in which the device is in the plantarflexion range of motion as illustrated in Figure D.1
Torque values are the magnitude of the forces and the direction is specified in Figure D.1 and in their corresponding header

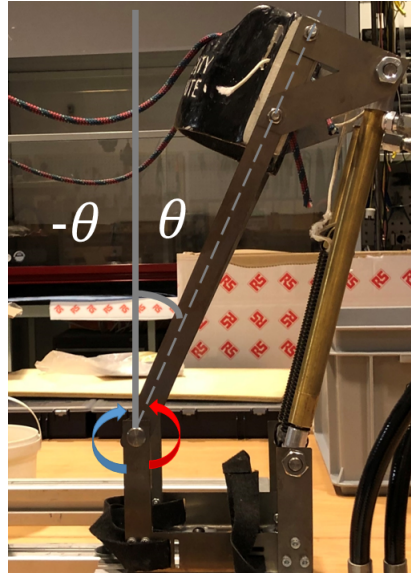


FIGURE D.1: Manual pump test angle and torque sign definition. Blue and red arrows are the dorsiflexion and plantarflexion torque direction respectively. A dorsiflexion torque is depicted as positive while a plantarflexion is negative. The grey solid line is the reference and the position at which the exoskeleton is neither performing plantarflexion nor dorsiflexion. The grey dotted line is the maximum dorsiflexion angle. Likewise, positive and negative angles represent the dorsiflexion and plantarflexion ROM.

D.2 Range of motion illustrations

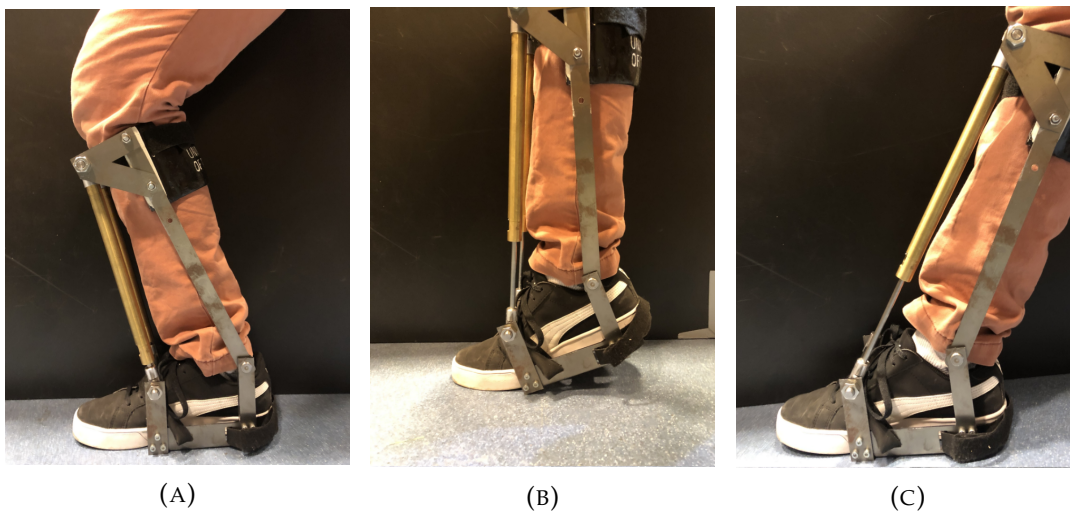


FIGURE D.2: Illustration of the device ROM being performed by a subject. (A) maximum dorsiflexion ROM, (B) subject's maximum natural stepping plantarflexion ROM of the, (C) and subject's maximum ankle plantarflexion ROM

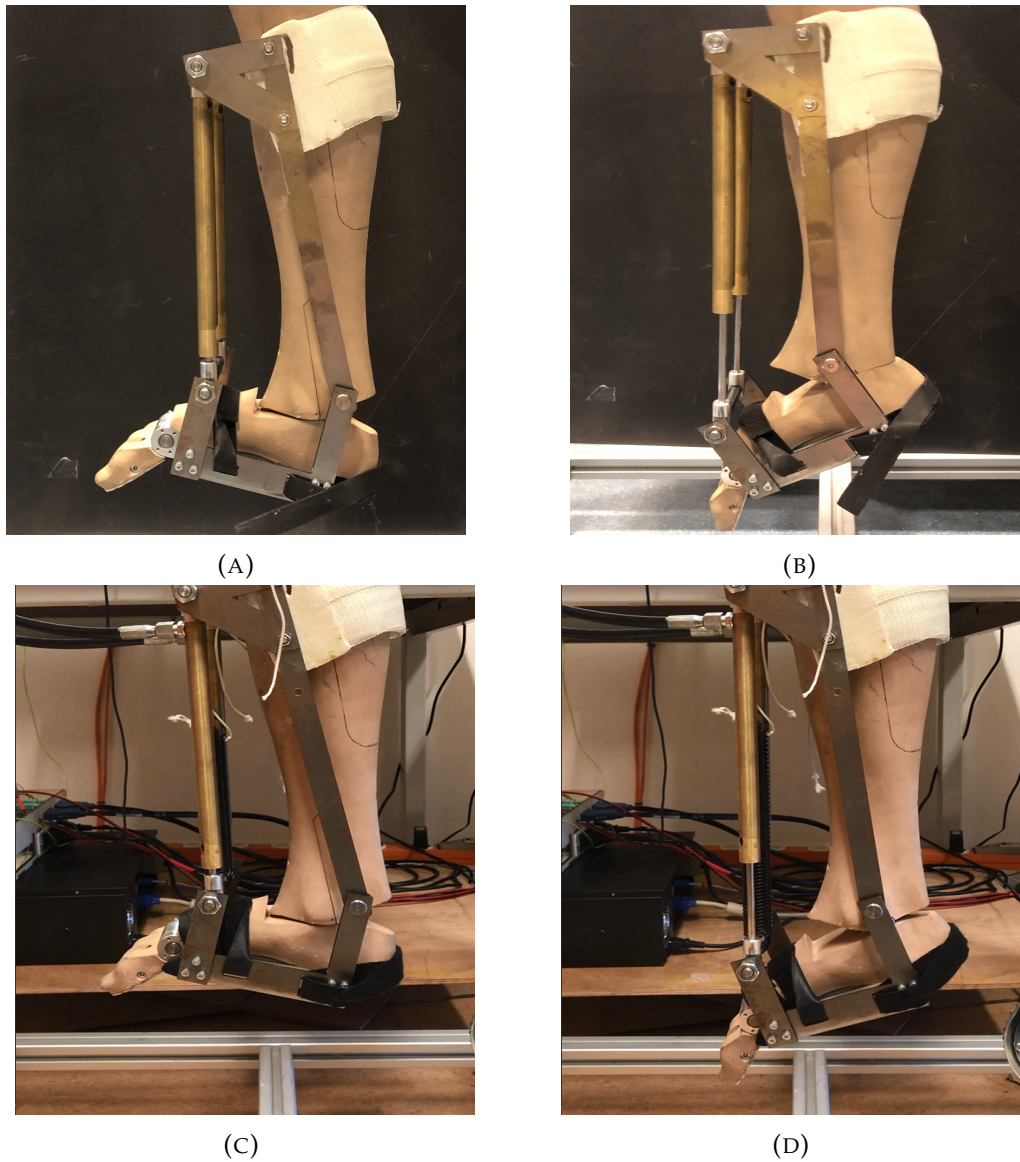


FIGURE D.3: (A) maximum dorsiflexion and (B) plantarflexion angle in the manual trial. (C) maximum dorsiflexion and (D) plantarflexion angle in the 480 mm/s velocity reference trial.